JHEP

Published for SISSA by Springer

Received: October 4, 2018
Revised: January 25, 2019
Accepted: February 11, 2019
Published: February 19, 2019

Right-handed neutrinos and R($D^{(*)}$)

Dean Robinson,[a] **Bibhushan Shakya**[a,b] **and Jure Zupan**[a]

[a] *Department of Physics, University of Cincinnati, Cincinnati, Ohio 45221, U.S.A.*

[b] *Leinweber Center for Theoretical Physics (LCTP), University of Michigan, Ann Arbor, Michigan 48109, U.S.A.*

E-mail: dean.robinson@uc.edu, shakyabn@ucmail.uc.edu, zupanje@ucmail.uc.edu

Abstract: We explore scenarios where the $R(D^{(*)})$ anomalies arise from semitauonic decays to a right-handed sterile neutrino. We perform an EFT study of all five simplified models capable of generating at tree-level the lowest dimension electroweak operators that give rise to this decay. We analyze their compatibility with current $R(D^{(*)})$ data and other relevant hadronic branching ratios, and show that one simplified model is excluded by this analysis. The remainder are compatible with collider constraints on the mediator semileptonic branching ratios, provided the mediator mass is of order TeV. We also discuss the phenomenology of the sterile neutrino itself, which includes possibilities for displaced decays at colliders and direct searches, measurable dark radiation, and gamma ray signals.

Keywords: Beyond Standard Model, Heavy Quark Physics, Neutrino Physics

ArXiv ePrint: 1807.04753

https://doi.org/10.1007/JHEP02(2019)119

JHEP02(2019)119

Contents

JHEP02(2019)119

1 Introduction

Measurements of the semitauonic to light semileptonic ratios at multiple experiments [1–6],

$$R(D^{(*)}) = \frac{\mathrm{Br}[\overline{B} \to D^{(*)}\tau\bar{\nu}]}{\mathrm{Br}[\overline{B} \to D^{(*)}l\bar{\nu}]}\,, \qquad l = e, \mu\,, \tag{1.1}$$

exhibit a 4σ tension with respect to the Standard Model (SM) predictions, once both D and D^* measurements are combined [7] (see also refs. [8–12]). Beyond the Standard Model (BSM) explanations of this anomaly typically require new physics (NP) close to the TeV scale. Since the SM neutrino is part of an electroweak doublet, corresponding constraints necessarily arise from high-p_T measurements of $pp \to \tau^+\tau^-$ at the LHC [13], Z and τ decays [14, 15], and contributions to flavor changing neutral currents (FCNCs), that can be severe.

As discussed in refs. [16, 17] (see also refs. [18, 19]), the observed enhancements of $R(D^{(*)})$ can be achieved not only through NP contributions to the $b \to c\tau\bar{\nu}_\tau$ decay, where

ν_τ is the SM left-handed τ neutrino, but also via a new decay channel, $b \to c\tau\bar{N}_R$, where N_R is a sterile right-handed neutrino. The $b \to c\tau\bar{\nu}$ decay becomes an incoherent sum of two contributions: to streamline notation we denote $\nu = N_R$ or ν_τ, so that $\mathrm{Br}[b \to c\tau\bar{\nu}] = \mathrm{Br}[b \to c\tau\bar{\nu}_\tau] + \mathrm{Br}[b \to c\tau\bar{N}_R]$. Since the NP couples to right-handed neutrinos, this can relax many of the electroweak constraints from the τ processes mentioned above.

In the specific context of refs. [16, 17], the $b \to c\tau\bar{N}_R$ decay is mediated by an $\mathrm{SU}(2)_L$ singlet W', which can be UV completed in a '3221' model. In this paper we generalize the EFT studies of refs. [16, 17] to the full set of dimension-six operators involving N_R (for earlier partial studies see [20–22]). Assuming that the NP corrections are due to a tree level exchange of a new mediator, there are five possible simplified models for $b \to c\tau\bar{N}_R$, whose mediators are: the $\mathrm{SU}(2)_L$-singlet vector boson — the W'; a scalar electroweak doublet; and three leptoquarks.

For each simplified model we identify which regions of parameter space are consistent with the $R(D^{(*)})$ anomaly, subject to exclusions from the $B_c \to \tau\nu$ branching ratio [23–25]. We further examine the variation in the signal differential distributions expected for each simplified model. While some electroweak constraints are relaxed, these simplified models nonetheless typically imply various sizeable semileptonic branching ratios for the tree-level mediators, for which moderately stringent collider bounds already exist. We show that, depending on the ratios of NP couplings in the simplified model, these in turn set lower bounds of $\mathcal{O}(\mathrm{TeV})$ on the mediator masses. We then proceed to examine the implications for neutrino phenomenology, such as bounds from radiative contributions to the SM neutrino masses, astrophysical constraints from sterile neutrino electromagnetic decays, plausible cosmological histories that admit these sterile neutrinos, and displaced decays at colliders and direct searches. In our analysis, we will require the N_R to be light — $m_{N_R} \lesssim \mathcal{O}(100)\,\mathrm{MeV}$ — in order not to disrupt the measured missing invariant mass spectrum in the full $\overline{B} \to D^{(*)}\tau\bar{\nu}$ decay chain. Whether heavier sterile neutrinos are compatible with data requires a dedicated forward-folded study, performed by the experimental collaborations.

The paper is structured as follows. Section 2 contains the EFT analysis of the $R(D^{(*)})$ data for the case of the right-handed neutrino and introduces the five possible tree-level mediators. Collider constraints on these simplified models are studied in section 3, while section 4 contains the related sterile neutrino phenomenology. Our conclusions follow in section 5. Appendix A examines the structure of the $b \to c\tau\bar{\nu}$ differential distributions for the simplified models.

2 EFT analysis

2.1 EFTs and simplified models

We consider the extension of the SM field content by a single new state, a right handed, sterile neutrino transforming as $N_R \sim (\mathbf{1}, \mathbf{1}, 0)$ under $\mathrm{SU}(3)_c \times \mathrm{SU}(2)_L \times \mathrm{U}(1)_Y$. This state may couple to the SM quarks via higher dimensional operators. Above the electroweak scale, one therefore adds to the renormalizable SM Lagrangian the following effective in-

JHEP02(2019)119

teractions,

$$\mathcal{L}_{\rm eff}^{\rm EW} = \sum_{a,d} \frac{C_{ad}}{\Lambda_{\rm eff}^{d-4}} Q_a + \cdots\,, \tag{2.1}$$

where Q_a are dimension-d operators, C_{ad} are the corresponding dimensionless Wilson coefficients (WCs), and $\Lambda_{\rm eff}$ is the effective scale defined to be

$$\Lambda_{\rm eff} = \left(2\sqrt{2}G_F V_{cb}\right)^{-1/2} \simeq 0.87 \left[\frac{40\times10^{-3}}{V_{cb}}\right]^{1/2} \text{TeV}\,. \tag{2.2}$$

The most general basis of dimension-6 operators that can generate the charged current $b \to c\tau\bar{N}_R$ decay is given by

$$Q_{\rm SR} = \epsilon_{ab}\big(\bar{Q}_L^a d_R\big)\big(\bar{L}_L^b N_R\big), \qquad Q_{\rm SL} = \big(\bar{u}_R Q_L^a\big)\big(\bar{L}_L^a N_R\big), \tag{2.3a}$$

$$Q_{\rm T} = \epsilon_{ab}\big(\bar{Q}_L^a \sigma^{\mu\nu} d_R\big)\big(\bar{L}_L^b \sigma_{\mu\nu} N_R\big), \qquad Q_{\rm VR} = \big(\bar{u}_R\gamma^\mu d_R\big)\big(\bar{\ell}_R\gamma_\mu N_R\big). \tag{2.3b}$$

Here a, b are $\mathrm{SU}(2)_L$ indices, ϵ_{ab} is an antisymmetric tensor with $\epsilon_{12} = -\epsilon_{21} = 1$, and we use the four-component notation, with Q_L the SM quark doublet, u_R and d_R the up- and down-quark singlets, and L_L the SM lepton doublet. (As usual, there is only one non-vanishing tensor operator, since $\sigma_{\mu\nu}P_L \otimes \sigma^{\mu\nu}P_R = 0$, which immediately follows from the relation $\sigma_{\mu\nu} \otimes \sigma^{\mu\nu}\gamma_5 = \sigma_{\mu\nu}\gamma_5 \otimes \sigma^{\mu\nu}$.) One may also include the dimension-8 operator

$$Q_{\rm VL} = \big(\bar{Q}_L \tilde{H}\gamma^\mu H^\dagger Q_L\big)\big(\bar{\ell}_R\gamma_\mu N_R\big), \tag{2.4}$$

where $\tilde{H} = \epsilon H^*$, as well as the operators with the left-handed sterile neutrino field, N_R^c, that start at dimension-7,

$$Q'_{\rm SR} = \big(\bar{Q}_L \tilde{H} d_R\big)\big(\bar{\ell}_R N_R^c\big), \qquad Q'_{\rm SL} = \big(\bar{u}_R H^\dagger Q_L\big)\big(\bar{\ell}_R N_R^c\big), \tag{2.5a}$$

$$Q'_{\rm T} = \big(\bar{u}_R \sigma^{\mu\nu} H^\dagger Q_L\big)\big(\bar{\ell}_R \sigma_{\mu\nu} N_R^c\big)\,, \qquad Q'_{\rm VR} = \big(\bar{u}_R\gamma^\mu d_R\big)\big(\bar{L}_L H\gamma_\mu N_R^c\big)\,, \tag{2.5b}$$

and the dimension-9 equivalent of $Q_{\rm VL}$,

$$Q'_{\rm VL} = \big(\bar{Q}_L \tilde{H}\gamma^\mu H^\dagger Q_L\big)\big(\bar{L}_L H\gamma_\mu N_R^c\big). \tag{2.6}$$

Each of the SM fields also carries a family index, i.e., Q_L^i, u_R^i, d_R^i, L_L^i, $i = 1, 2, 3$, and similarly for the Wilson coefficients, C_{ad}^{ijk}, and the operators, Q_{ad}^{ijk}, in eq. (2.1), which we have omitted for the sake of simplicity. Since we focus exclusively on the generation of $b \to c\tau\bar{\nu}$ decays below, we drop the family indices hereafter, unless otherwise stated. Consistency with bounds from direct searches requires that the Wilson coefficients in eq. (2.1) be at most $\mathcal{O}(1)$.

Below the electroweak scale, the top quark, the Higgs, and the W and Z bosons are integrated out. At the scale $\mu \sim m_{c,b}$, the effective Lagrangian, including SM terms (see, e.g., [26]), can be written

$$\mathcal{L}_{\rm eff} = \mathcal{L}_{\rm eff}^{\rm SM} + \frac{1}{\Lambda_{\rm eff}^2}\sum_i c_i \mathcal{O}_i\,, \tag{2.7}$$

JHEP02(2019)119

in which the NP contributions to $b \to c\tau\bar{\nu}$, induced by the dimension-6 operators in (2.3), are described by the following four-fermion operators,

$$\mathcal{O}_{\rm SR} = \big(\bar{c}_L b_R\big)\big(\bar{\tau}_L N_R\big), \qquad \mathcal{O}_{\rm SL} = \big(\bar{c}_R b_L\big)\big(\bar{\tau}_L N_R\big), \tag{2.8a}$$

$$\mathcal{O}_{\rm VR} = \big(\bar{c}_R \gamma^\mu b_R\big)\big(\bar{\tau}_R \gamma_\mu N_R\big), \qquad \mathcal{O}_{\rm T} = \big(\bar{c}_L \sigma^{\mu\nu} b_R\big)\big(\bar{\tau}_L \sigma_{\mu\nu} N_R\big). \tag{2.8b}$$

The scalar and tensor operators run under the Renormalization Group. The RG evolution from $M > m_t$ to $\mu < m_b$ gives at one-loop order in the leading log approximation for the Wilson coefficients at the low scale [27, 28], for $X = \mathrm{SR}, \mathrm{SL}, \mathrm{T}$,

$$\begin{aligned} c_X(\mu) &= \left[\frac{\alpha(m_b)}{\alpha(\mu)}\right]^{\gamma_X/2\beta_0^{(4)}} \left[\frac{\alpha(m_t)}{\alpha(m_b)}\right]^{\gamma_X/2\beta_0^{(5)}} \left[\frac{\alpha(M)}{\alpha(m_t)}\right]^{\gamma_X/2\beta_0^{(6)}} c_X(M) \\ &\equiv \rho_X(\mu; M) c_X(M)\,, \end{aligned} \tag{2.9}$$

with anomalous dimensions $\gamma_{\rm SR,SL} = -8$, $\gamma_{\rm T} = 8/3$ and the one loop β-function coefficient $\beta_0^{(n)} = 11 - 2n/3$. The running of $c_{\rm SR,SL,T}$ depends only weakly on the high scale M, and hereafter we set $M = \Lambda_{\rm eff}$. Fixing the scale low scale to $\mu = \sqrt{m_c m_b}$ — anticipating the chosen matching scale of QCD onto HQET for the $B \to D^{(*)}$ form factor parametrization — one finds

$$\rho_{\rm SR,SL} \simeq 1.7\,, \qquad \rho_{\rm T} \simeq 0.84\,. \tag{2.10}$$

Assuming the flavor indices are given in the mass eigenstate basis, the NP operators (2.1) can be matched onto the operators (2.3) as $c_X(\Lambda_{\rm eff}) = C_X^{233}$, neglecting the tiny mixing of active neutrinos into N_R. Note that the operators $\mathcal{O}_{\rm SR,T,SL}$ are accompanied by the $\mathrm{SU}(2)_L$ related operators

$$\mathcal{O}^s_{\rm SR} = \big(\bar{s}_L b_R\big)\big(\bar{\nu}_\tau N_R\big), \qquad \mathcal{O}^s_{\rm T} = \big(\bar{s}_L \sigma^{\mu\nu} b_R\big)\big(\bar{\nu}_\tau \sigma_{\mu\nu} N_R\big), \tag{2.11}$$

and $\big(\bar{c}_R t_L\big)\big(\bar{\nu}_\tau N_R\big)$. The Wilson coefficients of these operators, $c^s_{\rm SR,T,SL}$, correspond to $c_{\rm SR,T,SL}$, respectively, up to one-loop or higher-order corrections.

Each of the dimension-six operators in eq. (2.3) can arise from the tree level exchange of a new state, either a scalar or a vector. The possible mediators, together with the Wilson coefficients c_X they can contribute to, are listed in table 1. Two of these mediators are color singlets: the charged vector resonance W'_μ, discussed extensively in refs. [16, 17], and the weak doublet scalar Φ. The remaining mediators are leptoquarks, for which we use the notation from ref. [29]. In some cases the structure of the mediator Lagrangian, $\delta\mathcal{L}_{\rm int}$, implies relations between the various Wilson coefficients, denoted by equalities in table 1. In particular, for the $\tilde{R}_2$ and S_1 models, $c_{\rm SR}(\Lambda_{\rm eff}) = \pm 4 c_{\rm T}(\Lambda_{\rm eff})$, which evolves to

$$c_{\rm SR}(\mu) = \pm 4 r\, c_{\rm T}(\mu)\,, \qquad r \equiv \rho_{\rm SR}/\rho_{\rm T} \simeq 2.0\,, \tag{2.12}$$

at the B meson scale.

For completeness, we list the remaining $b \to c\tau\bar{N}_R$ dimension-6 operators at $\mu \sim m_{c,b}$,

$$\mathcal{O}'_{\rm SR} = \big(\bar{c}_L b_R\big)\big(\bar{\tau}_R N_R^c\big), \qquad \mathcal{O}'_{\rm SL} = \big(\bar{c}_R b_L\big)\big(\bar{\tau}_R N_R^c\big), \tag{2.13a}$$

$$\mathcal{O}'_{\rm VR} = \big(\bar{c}_R \gamma^\mu b_R\big)\big(\bar{\tau}_L \gamma_\mu N_R^c\big), \qquad \mathcal{O}'_{\rm VL} = \big(\bar{c}_L \gamma^\mu b_L\big)\big(\bar{\tau}_L \gamma_\mu N_R^c\big), \tag{2.13b}$$

$$\mathcal{O}'_{\rm T} = \big(\bar{c}_R \sigma^{\mu\nu} b_L\big)\big(\bar{\tau}_R \sigma_{\mu\nu} N_R^c\big), \qquad \mathcal{O}_{\rm VL} = \big(\bar{c}_L \gamma^\mu b_L\big)\big(\bar{\tau}_R \gamma_\mu N_R\big). \tag{2.13c}$$

JHEP02(2019)119

mediator	irrep	$\delta\mathcal{L}_{\text{int}}$	WCs
W'_μ	$(1,1)_1$	$g'\big(c_q\bar{u}_R\gamma_\mu d_R + c_N\bar{\ell}_R\gamma_\mu N_R\big)W'^\mu$	c_{VR}
Φ	$(1,2)_{1/2}$	$y_u\bar{u}_R Q_L\epsilon\Phi + y_d\bar{d}_R Q_L\Phi^\dagger + y_N\bar{N}_R L_L\epsilon\Phi$	$c_{\text{SL}}(\mu)$, $c_{\text{SR}}(\mu)$
U_1^μ	$(3,1)_{2/3}$	$\big(\alpha_{LQ}\bar{L}_L\gamma_\mu Q_L + \alpha_{\ell d}\bar{\ell}_R\gamma_\mu d_R\big)U_1^{\mu\dagger} + \alpha_{uN}\big(\bar{u}_R\gamma_\mu N_R\big)U_1^\mu$	$c_{\text{SL}}(\mu)$, c_{VR}
$\tilde{R}_2$	$(3,2)_{1/6}$	$\alpha_{Ld}\big(\bar{L}_L d_R\big)\epsilon\tilde{R}_2^\dagger + \alpha_{QN}\big(\bar{Q}_L N_R\big)\tilde{R}_2$	$c_{\text{SR}}(\mu) = 4rc_{\text{T}}(\mu)$
S_1	$(\bar{3},1)_{1/3}$	$z_u(\bar{U}_R^c\ell_R)S_1 + z_d(\bar{d}_R^c N_R)S_1 + z_Q(\bar{Q}_L^c\epsilon L_L)S_1$	c_{VR}, $c_{\text{SR}}(\mu) = -4rc_{\text{T}}(\mu)$

Table 1. The tree-level mediators that can generate the four-fermion operators with right-handed neutrino, N_R, in eqs. (2.8). The relevant Wilson coefficients are shown in the final column, explicitly defined at scale μ where relevant, and including the factor $r \equiv \rho_{\text{SR}}/\rho_{\text{T}} \simeq 2.0$.

The generation of these operators from the electroweak scale four-Fermi operators (2.4)–(2.6) requires additional insertions of the Higgs vev, v_{EW}, and, apart from $\mathcal{O}_{\text{VL}}$, also the left-handed sterile neutrino N_R^c. These $\mathcal{O}'_a$ operators are the same as those in ref. [27], but with N_R^c replacing the SM neutrino ν_τ. Eqs. (2.8) and (2.13) together form a complete basis of $b \to c\tau\bar{N}_R$ dimension-six four-fermion operators. Since the Wilson coefficients of the operators in eq. (2.13) are suppressed by additional powers of $v_{\text{EW}}/\Lambda_{\text{eff}}$, we will only focus on the dimension-6 operators listed in eq. (2.3) and (2.8) in the remainder of this paper.

2.2 Fits to $R(D^{(*)})$ data

The present experimental world-averages for $R(D^{(*)})$ are [7]

$$R(D)\big|_{\text{exp}} = 0.407 \pm 0.046\,, \qquad R(D^*)\big|_{\text{exp}} = 0.304 \pm 0.015\,, \qquad \text{corr.} = -0.20\,. \tag{2.14}$$

The SM predictions, e.g. making use of the model-independent form factor fit '$L_{w\geq 1}$+SR' of ref. [8] (see also refs. [9, 10]), are

$$R(D)\big|_{\text{th}} = 0.299 \pm 0.003, \qquad R(D^*)\big|_{\text{th}} = 0.257 \pm 0.003, \qquad \text{corr.} = +0.44\,. \tag{2.15}$$

With the addition of a right-handed neutrino decay mode, the $\overline{B} \to D^{(*)}\tau\bar{\nu}$ decays become an incoherent sum of two contributions: the SM decay $b \to c\tau\bar{\nu}_\tau$ and the new mode $b \to c\tau\bar{N}_R$. The N_R contributions therefore increase both of the $\overline{B} \to D^{(*)}\tau\bar{\nu}$ branching ratios above the SM predictions, as would be required to explain the experimental measurements of $R(D^{(*)})$.

In figure 1, we show for each simplified model of table 1 the accessible contours or regions in the $R(D) - R(D^*)$ plane, compared to the experimental data. The predictions for NP corrections to $R(D^{(*)})$ are obtained from the expressions in ref. [30], making use of the form factor fit '$L_{w\geq 1}$+SR' of ref. [8]. This fit was performed at next-to-leading order in the heavy quark expansion, with matching scale $\mu = \sqrt{m_b m_c}$ and quark masses defined

JHEP02(2019)119

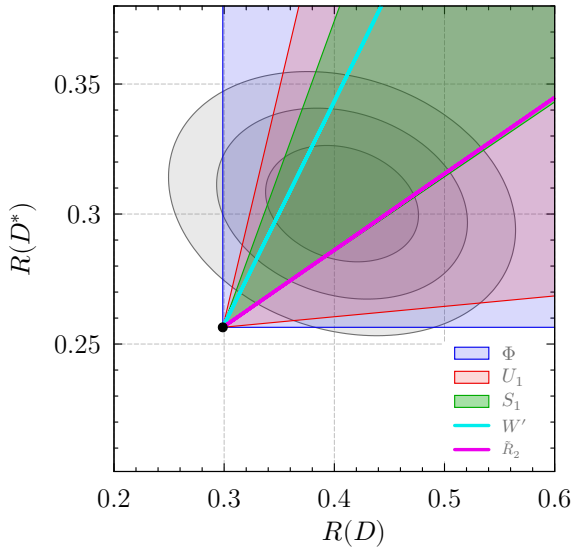

Figure 1. The enhancements of $R(D^{(*)})$ from $b \to c\tau\bar{N}_R$ decays for various simplified models. The world average experimental 1σ, 2σ, and 3σ fit regions are shown in decreasing shade of gray. The SM point is denoted by a black dot.

in the $\Upsilon(1S)$ scheme, relevant for a self-consistent treatment of the $B_c \to \tau\nu$ constraints below. The W' and $\tilde{R}_2$ simplified models have only a single free Wilson coefficient and are constrained to a contour: since the N_R contributions add incoherently to the SM, the phase of each Wilson coefficient is unphysical. By contrast, Φ, U_1, and S_1 have two free Wilson coefficients, corresponding to two free magnitudes and a physical relative phase, permitting them to span a region.

Assuming first that all Wilson coefficients are real, we show in figure 2 the 0.5σ, 1σ CLs (dark, light blue) and 1.5σ, 2σ CLs (dark, light green) in the relevant Wilson coefficient spaces for each simplified model. These CLs are generated by the χ^2 defined with respect to the $R(D^{(*)})$ experimental data and correlations (2.14), not including the possible effects of NP errors. That is,

$$\chi^2 = \boldsymbol{v}^T \sigma^{-1}_{R(D^{(*)})} \boldsymbol{v}\,, \qquad \boldsymbol{v} = \big(R(D)_{\rm th} - R(D)_{\rm exp}\,, R(D^*)_{\rm th} - R(D^*)_{\rm exp}\big)\,, \tag{2.16}$$

The χ^2 CLs (dof =2) in figure 2 then correspond simply to projections of the CL ellipses in figure 1. We will hereafter refer to the minimal χ^2 points in the WC space for each simplified model as the model's 'best fit' points with respect to the $R(D^{(*)})$ results (2.14), though it should be emphasized that this is not the same as a NP WC fit to the experimental data, which would require inclusion of the NP errors in the underlying experimental fits. In figure 2 the best fit points are shown by black dots, with explicit values provided in table 2. For the W' and $\tilde{R}_2$ models, we show the explicit χ^2, as well as the intervals corresponding to 1σ and 2σ CLs (dof = 2).

The additional NP currents from the operators (2.8) also incoherently modify the $B_c \to \tau\nu$ decay rate with respect to the SM contribution (cf. refs. [23, 24]), such that

$$\mathrm{Br}(B_c \to \tau\nu) = \frac{\tau_{B_c} f_{B_c}^2 m_{B_c} m_\tau^2}{64\pi\Lambda_{\rm eff}^4} \left(1 - m_\tau^2/m_{B_c}^2\right)^2 \left[1 + \left| c_{\rm VR} + \frac{m_{B_c}^2 (c_{\rm SL}^{(\mu)} - c_{\rm SR}^{(\mu)})}{m_\tau(\overline{m}_b + \overline{m}_c)} \right|^2\right]\,, \tag{2.17}$$

JHEP02(2019)119

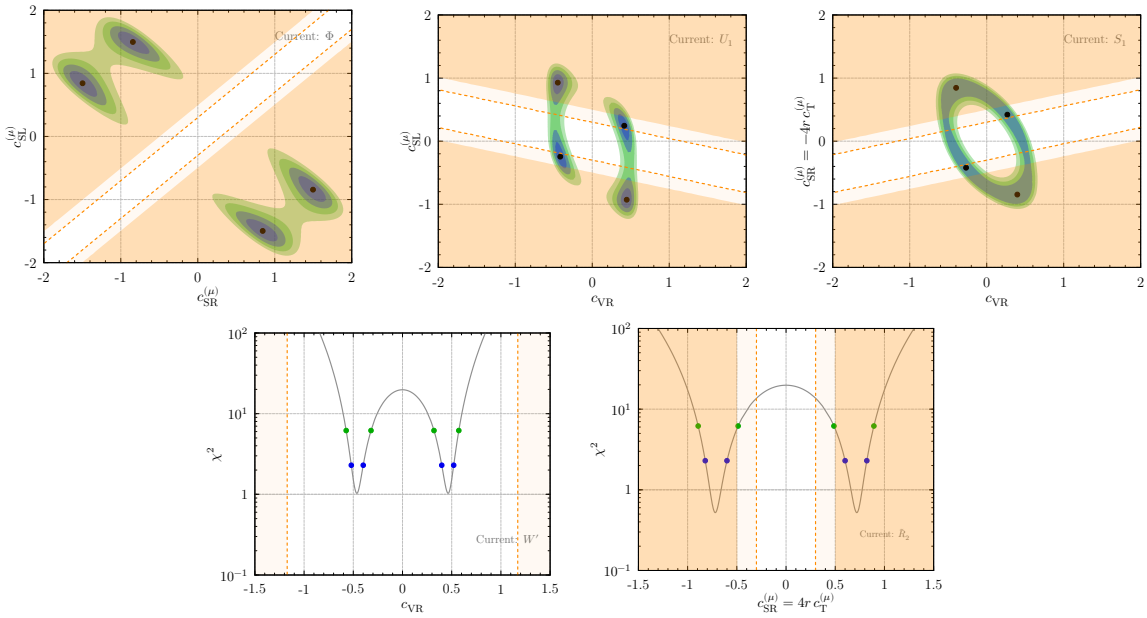

Figure 2. *Top*: the fit regions for Φ, U_1, and S_1 models with respect to the $R(D^{(*)})$ results (2.14) in the relevant Wilson coefficient spaces, assuming that all Wilson coefficients are real. Shown are 0.5σ, 1σ CLs (dark, light blue) and 1.5σ, 2σ CLs (dark, light green). Best fit points are shown by black dots. *Bottom*: the χ^2 (dof = 2) for the W' and $\tilde{R}_2$ models in the relevant Wilson coefficient space. The 1σ and 2σ CLs are shown by blue and green dots, respectively. Also shown are $B_c \to \tau\nu$ exclusion regions requiring $\mathrm{Br}[B_c \to \tau\nu] < 10\%$ (dark orange). For a sense of scaling, a more aggressive $\mathrm{Br}[B_c \to \tau\nu] < 5\%$ exclusion region is demarcated by a dashed orange line.

in which $f_{B_c} \simeq 0.43\,\mathrm{GeV}$ [31] and $\tau_{B_c} \simeq 0.507\,\mathrm{ps}$ [32], and $\overline{m}_{c,b}$ are the $\overline{\mathrm{MS}}$ quark masses, obeying $m_Q \simeq \overline{m}_Q(1 + \alpha_s/\pi[4/3 - \ln(m_Q^2/\mu^2)])$. Self-consistency with the form factor treatment of ref. [8] requires these masses to be evaluated at $\mu = \sqrt{m_b m_c}$ in the $\Upsilon(1S)$ quark mass scheme. In figure 2 we show the corresponding exclusion regions for the relevant Wilson coefficient spaces (shaded orange), requiring $\mathrm{Br}(B_c \to \tau\bar{\nu}) < 10\%$ [23, 24]. For a sense of scaling, we also include a more aggressive $\mathrm{Br}(B_c \to \tau\bar{\nu}) < 5\%$ exclusion demarcated by a dashed orange line. One sees that the Φ simplified model is excluded, while the $\tilde{R}_2$ 2σ CL is not quite excluded by the $\mathrm{Br}(B_c \to \tau\bar{\nu}) < 10\%$ constraint. The U_1 and S_1 best fit points are in mild tension with the aggressive $\mathrm{Br}(B_c \to \tau\bar{\nu}) < 5\%$ exclusion, but also exhibit allowed regions for their 1σ CLs.

Lifting the requirement of real Wilson coefficients, the Φ, U_1, and S_1 models now have a physical phase and inhabit a three dimensional parameter space: two Wilson coefficient magnitudes, schematically denoted $|c_{1,2}|$, and a relative phase φ. For the basis of Wilson coefficients defined by the N_R operators (2.8), however, the amplitudes for the $\overline{B} \to D^{(*)} l\bar{\nu}$ decay alone have no physical relative phases. (Physical phases do exist once the D^* and τ decay amplitudes are included.) Consequently, for a given choice of $|c_{1,2}|$, there may exist a nontrivial value for $\cos\varphi$ that minimizes the χ^2 for $R(D^{(*)})$ in eq. (2.16). We refer to this scenario as the 'phase optimized' case, denoted $\varphi = \varphi_0(|c_1|, |c_2|)$. In explicit numerical terms, for the form factor and $R(D^{(*)})$ inputs described above, the Φ, U_1, and S_1 models

JHEP02(2019)119

Model	WCs	Real		Phase-optimized	
		Best fit	χ^2	Best fit	χ^2
W'	$c_{\rm VR}$	± 0.46	1.0	—	—
$\tilde{R}_2$	$c_{\rm SR}^{(\mu)} = 4r\, c_{\rm T}^{(\mu)}$	± 0.72	0.5	—	—
Φ	$\{c_{\rm SR}^{(\mu)}, c_{\rm SL}^{(\mu)}\}$	$\{\pm 1.50, \mp 0.84\}$	0.	$\{1.50, -0.84\}$	0.
				$\{1.21, \pm 1.21 e^{\pm i 0.17\pi}\}$	0.
		$\{\pm 0.84, \mp 1.50\}$	0.	$\{0.84, -1.50\}$	0.
U_1	$\{c_{\rm VR}, c_{\rm SL}^{(\mu)}\}$	$\{\pm 0.45, \mp 0.93\}$	0.	$\{0.45, -0.93\}$	0.
		$\{\pm 0.42, \pm 0.24\}$	0.	$\{0.42, 0.24\}$	0.
S_1	$\{c_{\rm VR},$	$\{\pm 0.40, \mp 0.85\}$	0.	$\{0.40, -0.85\}$	0.
	$c_{\rm SR}^{(\mu)} = -4r\, c_{\rm T}^{(\mu)}\}$	$\{\pm 0.27, \pm 0.42\}$	0.	$\{0.27, 0.42\}$	0.

Table 2. Best fit points for each model with respect to the $R(D^{(*)})$ results (2.14), for real and phase-optimized Wilson coefficients. In the phase-optimized case, we show best fits up to an overall phase, by choosing the first WC to be real and positive definite.

have non-trivial solutions

$$\cos(\varphi_0) = \begin{cases} \frac{0.24 - 0.51|c_{\rm SR}|^2 - 0.51|c_{\rm SL}|^2}{|c_{\rm SR}||c_{\rm SL}|}\,, & \Phi\,, \\ \frac{0.38 - 1.38|c_{\rm VR}|^2 - 0.60|c_{\rm SL}|^2}{|c_{\rm VR}||c_{\rm SL}|}\,, & U_1\,, \\ \frac{0.32 - 1.40|c_{\rm VR}|^2 - 0.61|c_{\rm SR}|^2}{|c_{\rm VR}||c_{\rm SR}|}\,, & S_1\,, \end{cases} \tag{2.18}$$

valid only on the domain $|\cos(\varphi_0)| < 1$, and otherwise $\cos(\varphi_0) = \pm 1$. These phase-optimized CLs for the Φ, U_1, and S_1 models are shown in figure 3, with the explicit best fit points listed in table 2. The best fit points for U_1 and S_1 remain the same, and one sees that these models continue to have non-excluded 1σ CLs. An additional best fit point emerges for the Φ simplified model; however, this model remains excluded, and we therefore do not consider it further in this paper.

Finally, the exchange of mediators that generates the $c_{\rm SR,T}$ Wilson coefficients also results in $c^s_{\rm SR,T}$ of similar size (see eq. (2.11)). The two operators in eq. (2.11) contribute to $b \to s\nu\bar{\nu}$ rates. This gives, for instance, for the $B \to K\nu\bar{\nu}$ decay rate (far enough from the kinematic threshold so that we can neglect all the final state masses) [33, 34]

$$\begin{aligned} \frac{d\Gamma_{B\to K\nu\bar{\nu}}}{dz} \Big/ \frac{d\Gamma_{B\to K\nu\bar{\nu}}}{dz}\Big|_{\rm SM} &= 1 + z\frac{32\pi^2}{3\alpha^2}\left|\frac{V_{cb}}{C^{\rm SM}_{\nu\nu} V_{tb} V^*_{ts}}\right|^2 \left[\frac{3}{8}\frac{(c^s_{\rm SR})^2}{(1-z)^2}\frac{f_0^2}{f_+^2} + (c^s_{\rm T})^2\frac{f_T^2}{f_+^2}\right] \\ &\simeq 1 + 5\times 10^4\, z\left[\frac{3}{8}\frac{(c^s_{\rm SR})^2}{(1-z)^2}\frac{f_0^2}{f_+^2} + (c^s_{\rm T})^2\frac{f_T^2}{f_+^2}\right], \end{aligned} \tag{2.19}$$

JHEP02(2019)119

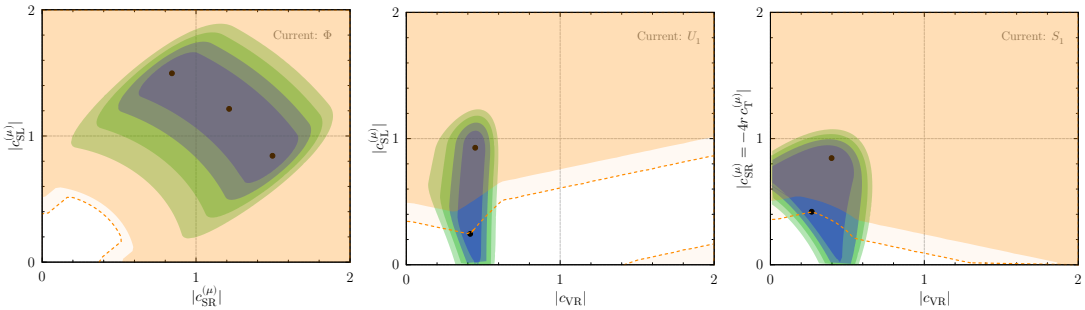

Figure 3. The phase-optimized CLs with respect to the $R(D^{(*)})$ results (2.14) for Φ, U_1, and S_1 models in the relevant Wilson coefficient spaces, imposing the condition $\varphi = \varphi_0(|c_1|, |c_2|)$. Shown are 0.5σ, 1σ CLs (dark, light blue) and 1.5σ, 2σ CLs (dark, light green). Also shown are $B_c \to \tau\nu$ exclusion regions requiring $\mathrm{Br}[B_c \to \tau\nu] < 10\%$ (dark orange). For a sense of scaling, a more aggressive $\mathrm{Br}[B_c \to \tau\nu] < 5\%$ exclusion region is demarcated by a dashed orange line. Best fit points are shown by black dots.

with the three $B \to K$ form factors, $f_0(q^2)$, $f_+(q^2)$, $f_T(q^2)$, functions of q^2, the invariant mass squared of the neutrino pair, and $z = q^2/m_B^2$. The present experimental bound, $Br(B^+ \to K^+\nu\bar{\nu}) < 1.6 \times 10^{-5}$ [35], is only a factor of a few above the SM prediction, $Br(B^+ \to K^+\nu\bar{\nu})|_{\rm SM} \simeq 4 \times 10^{-6}$ [36]. This implies that $c_{\rm SR}^s$ and $c_{\rm T}^s$ are highly suppressed, to the level of $\mathcal{O}(10^{-2})$, introducing tensions with the required size of $c_{\rm SR}, c_{\rm T}$ to explain the $R(D^{(*)})$ anomaly. In the single mediator exchange models in table 1, this means that the product $\alpha_{Ld}^3 \alpha_{QN}^2$ for $\tilde{R}_2$ and the product $z_d^3 z_Q^2$ for S_1 (and y_d^{32} for Φ) need to be much smaller than what is required to explain $R(D^{(*)})$. This excludes the $\tilde{R}_2$ as a simple one mediator solution to $R(D^{(*)})$: additional operators coupling to the second generation of quark doublets must be introduced, whose couplings are tuned appropriately to suppress the contributions to $b \to s\nu\bar{\nu}$. However, this approach would in turn induce large radiative contributions to the neutrino masses, which would also need to be tuned away (see section 4). The S_1 model also generates too large a $b \to s\nu\bar{\nu}$ transition rate at the (non-excluded) best fit point, where $c_{\rm SR}$ and $c_{\rm T}$ are nonzero. The dangerous $b \to s\nu\bar{\nu}$ contribution can be suppressed by taking $z_Q^{23} \to 0$ (see table 1), which forces $c_{\rm SR} = c_{\rm T} \to 0$. This $c_{\rm SR} = c_{\rm T} = 0$ point leads to only a small change in χ^2, corresponding to a less than $0.5\,\sigma$ shift in significance, see figure 2.

2.3 Differential distributions

The reliability of the above $R(D^{(*)})$ fit results turns upon the underlying assumption that the differential distributions, and hence experimental acceptances, of the $\overline{B} \to D^{(*)}\tau\bar{\nu}$ decays are not significantly modified in the presence of the NP currents. The $\overline{B} \to D^{(*)}\tau\bar{\nu}$ branching ratios are extracted from a simultaneous float of background and signal data, so that significant modification of the acceptances versus the SM template may alter the extracted values.

To estimate the size of these potential effects, we examine the cascades $\overline{B} \to (D^* \to D\pi)(\tau \to \ell\bar{\nu}_\ell\nu_\tau)\bar{\nu}$ and $\overline{B} \to D(\tau \to \ell\nu\nu)\nu$, comparing the purely SM predictions with the predictions for the 2σ fit regions of the simplified models. We take N_R to be massless, and

JHEP02(2019)119

include the phase space cuts,

$$q^2 = (p_B - p_{D^{(*)}})^2 > 4 \text{ GeV}^2\,, \qquad E_\ell > 400 \text{ MeV}\,, \qquad m^2_{\text{miss}} > 1.5 \text{ GeV}^2\,, \tag{2.20}$$

as an approximate simulation of the BaBar and Belle measurements performed in refs. [2, 3]. These distributions are generated as in ref. [30], using a preliminary version of the `Hammer` library [37]. In appendix A we show the variation of the normalized differential distributions over the 2σ fit regions in figure 2 — i.e. assuming real couplings, for simplicity — for the detector observables E_D, E_ℓ, m^2_{miss}, $\cos\theta_{D\ell}$ and q^2 compared to the SM distributions.

As already found in ref. [17], the variation of the W' model with respect to the SM is negligible. However, the $\tilde{R}_2$, U_1 and S_1 theories, since they include interfering scalar and/or tensor currents, may significantly modify the spectra, as seen also in ref. [30] for the NP tensor current coupling to a SM neutrino. Thus, a fully self-consistent $R(D^{(*)})$ fit for these models will require a forward-folded analysis by the experimental collaborations: our analysis above and CLs should be taken only as an approximate guide, within likely 1σ variations in the values of $R(D^{(*)})$.

3 Collider constraints on simplified models

The simplified models are subject to low energy flavor constraints as well as bounds from collider searches. These depend crucially on the assumed flavor structure of the couplings in table 1. Furthermore, the sensitivity of the collider searches depend on other open decay channels of the mediators. In this section, we discuss these constraints for the simplified models.

For the S_1 and $\tilde{R}_2$ models, the best fit points are naively excluded by bounds on $b \to s\nu\bar{\nu}$ transitions. These can be avoided by including higher dimensional operators, due to a new set of heavy states, inevitably introducing greater model dependence for LHC studies. To remain as model independent as possible, we study the collider signatures for these models using their ($B_c \to \tau\nu$ consistent) best fit points for $R(D^{(*)})$ as a benchmark, assuming that any new fields required to ameliorate large $b \to s\nu\bar{\nu}$ (and/or large neutrino mass contributions) are sufficiently heavy that they do not affect mediator production or decay.

3.1 W' coupling to right-handed SM fermions

The charged vector boson W'_μ couples to $\text{SU}(2)_L$ singlets only, and transforms as $W'_\mu \sim (1,1)_1$, with

$$\mathcal{L} = \frac{g_V}{\sqrt{2}} c_q^{ij}\, \bar{u}^i_R \not{W}' d^j_R + \frac{g_V}{\sqrt{2}} c^i_N \bar{\ell}^i_R \not{W}' N_R + \text{h.c.}, \tag{3.1}$$

where $i,j = 1,2,3$ are generational indices. As in table 1, the coefficients c_q^{ij} and c^i_N encode the flavor structure of the interactions, while g_V is the overall coupling strength (in simple gauge models for W' it can be identified with the gauge coupling constant [16, 17]). A tree level exchange of W' generates the operator $\mathcal{O}_{\text{VR}}$, cf. eqs. (2.8b) and (2.7), with

$$\frac{c_{\text{VR}}}{\Lambda^2_{\text{eff}}} = -\frac{g_V^2 c_q^{23} c_N^3}{2 m^2_{W'}}. \tag{3.2}$$

JHEP02(2019)119

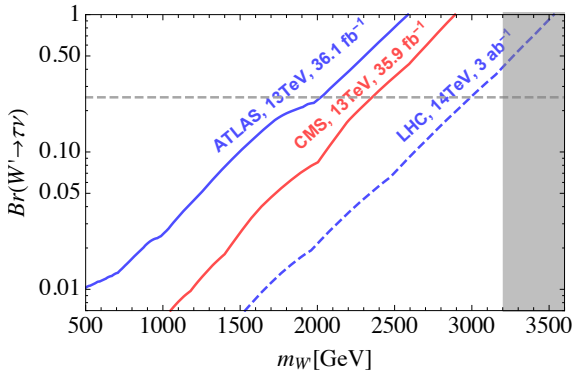

Figure 4. The bound on $Br(W' \to \tau\nu)$ as a function of W' mass from the 13 TeV ATLAS [38] (solid blue) and CMS [39] (solid red) searches, as well as the projected reach at the end of the high-luminosity LHC run (dashed blue), for the case $c_q^{23} = c_N^3$, W' mass given by eq. (3.3) to fit to $R(D^{(*)})$ data, and the W' couplings to all the other SM quarks set to zero. In this case $Br(W' \to \tau\nu) = 0.25$ (dashed grey line) if no other W' decay channels are open. All the bounds assume narrow width for W'. The region excluded by unitarity is shaded in grey.

The best fit values for $c_{\rm VR}$ in table 2 then imply [17]

$$m_{W'} \simeq 540 \left| c_q^{23} c_N^3 \right|^{1/2} \left[\frac{g_V}{0.6} \right] \left[\frac{40 \times 10^{-3}}{V_{cb}} \right]^{1/2} \text{GeV} \,. \tag{3.3}$$

In figure 4 we show the minimal set of experimental constraints on such models, applicable to the simplified W' model. For this plot we set $c_q^{23} = c_N^3$, take eq. (3.3) to provide the W' mass that fits the $R(D^{(*)})$ data, and set the W' couplings to all other SM quarks to zero. For this scenario, the ATLAS search at 13 TeV with 36.1 fb^{-1} luminosity [38] and the CMS search with 35.9 fb^{-1} [39] convert to a 95% CL bounds on Br$(W' \to \tau\nu)$ shown in figure 4 (blue and red lines, respectively), see also refs. [40, 41] for previous bounds. The dashed blue line denotes a naive extrapolation of the expected bound from ref. [38] to the end of the high-luminosity LHC Run 5, assuming 3000 fb^{-1} integrated luminosity at 14 TeV. For $c_q^{23} = c_N^3$ the two branching ratios of W' are Br$(W' \to \tau\nu)$: Br$(W' \to 2j) \simeq 1 : 3$; the former is denoted by the horizontal grey dashed line in figure 4. The two branching ratios can be correspondingly smaller if other decay channels are open (for instance, to extra vector-like fermions, as contemplated in refs. [16, 17]). The grey shaded region is excluded by unitarity, which constrains $3(c_q^{23})^2 + (c_N^3)^2 < 16\pi/g_V^2$ [42]. The experimental bounds shown in figure 4 assume that the W' has a narrow width. This assumption fails for heavy W' with a mass in the few TeV range. According to the results of a recast of the CMS search [39] performed for a wide W' [43], the entire perturbative parameter space of the W' model is excluded, except potentially for the very light W', with masses below 500 GeV, where a reanalysis of older experiments would need to be carefully performed. Bounds on W' from di-jet production [44–48] are less stringent and are not relevant for this simplified model.

Since the W'_μ couples to right-handed quarks, there is significant freedom in terms of the flavor structure of the c_q^{ij} and c_N^i couplings. We have limited the discussion to the

JHEP02(2019)119

minimal case, taking only $c_q^{23}, c_N^3 \neq 0$, which is non-generic but possible, for instance, in flavor-locked models [17, 49]. In most flavor models all the c_q^{ij}, c_N^i are non-zero, leading to constraints from precision measurements. In UV completions (see refs. [16, 17]), the W' boson is expected to be accompanied by a Z' state. The Z' can, however, be parametrically heavier than the W', in particular if additional sources of symmetry breaking are present. The collider constraints on W' and Z' are often comparable, while the flavor constraints from FCNCs are far more stringent for Z' in the presence of any appreciable off-diagonal couplings [17]: contributions from W' exchange to flavor changing neutral currents only arise at one-loop and are significantly less constraining.

3.2 Vector leptoquark U_1^μ

The interaction Lagrangian for the $U_1^\mu \sim (3,1)_{2/3}$ vector leptoquark is

$$\mathcal{L} \supset \alpha_{LQ}^{ij}(\bar{L}_L^i \gamma_\mu Q_L^j) U_1^{\mu\dagger} + \alpha_{\ell d}^{ij}(\bar{\ell}_R^i \gamma_\mu d_R^j) U_1^{\mu\dagger} + \alpha_{uN}^i(\bar{u}_R^i \gamma_\mu N_R) U_1^\mu + \text{h.c.}, \tag{3.4}$$

while the kinetic term, following the notation in [50], is

$$\mathcal{L} \supset -\frac{1}{2} U_{1\mu\nu}^\dagger U^{\mu\nu} + m_{U_1}^2 U_{1\mu}^\dagger U_1^\mu - i g_s \kappa U_{1\mu}^\dagger T^a U_{1\nu} G^{a\mu\nu}, \tag{3.5}$$

with $U_{\mu\nu} = D_\mu U_{1\nu} - D_\nu U_{1\mu}$ the field strength tensor, and κ a dimensionless coupling.

When the leptoquark is integrated out, eq. (3.4) gives two four-fermion operators, relevant for $R(D^{(*)})$ anomalies, with the Wilson coefficients

$$\frac{c_{\text{SL}}^{(\mu)}}{\rho_{\text{SL}} \Lambda_{\text{eff}}^2} = 2\frac{\alpha_{LQ}^{33}\alpha_{uN}^2}{m_{U_1}^2}, \qquad \frac{c_{\text{VR}}}{\Lambda_{\text{eff}}^2} = -\frac{\alpha_{\ell d}^{33}\alpha_{uN}^2}{m_{U_1}^2}. \tag{3.6}$$

The best fit values for the U_1 WCs in table 2 then imply

$$m_{U_1} \simeq 3.2 \left|\alpha_{LQ}^{33}\alpha_{uN}^2\right|^{1/2} \left[\frac{40 \times 10^{-3}}{V_{cb}}\right]^{1/2} \text{TeV}\,, \tag{3.7}$$

with

$$\alpha_{\ell d}^{33} \simeq -5.8\, \alpha_{LQ}^{33}, \tag{3.8}$$

where we used the lower set of best fits for U_1 in table 2 (the upper set is excluded by $B_c \to \tau\nu$, see figure 2). If one instead sets $c_{\text{SL}} = 0$, the best fit simply maps onto the W' result (since both models then have the same non-zero coupling c_{VR}): $|c_{\text{VR}}| \simeq 0.46$, and

$$m_{U_1} \simeq 1.3 \left|\alpha_{\ell d}^{33}\alpha_{uN}^2\right|^{1/2} \left[\frac{40 \times 10^{-3}}{V_{cb}}\right]^{1/2} \text{TeV}\,. \tag{3.9}$$

At the LHC, the U_1 leptoquark can be singly or pair produced. The pair production, $pp \to U_1 U_1^\dagger$, proceeds through gluon fusion, via the color octet term in (3.5), for which we take $\kappa = 1$ following ref. [51]. The collider signatures of U_1 pair production depend on the

JHEP02(2019)119

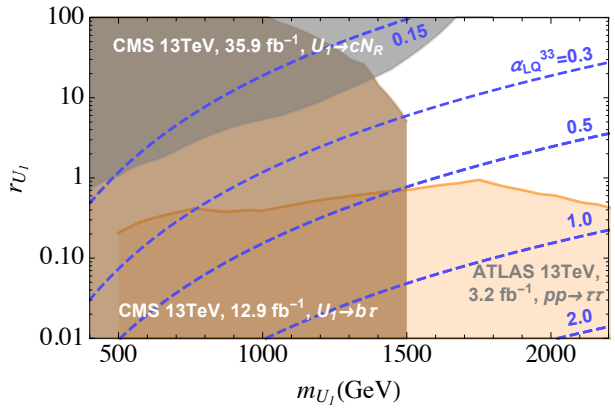

Figure 5. The LHC bounds from [51] (grey), [52] (brown), and [13, 53] (orange) on the U_1^μ vector leptoquark mass, assuming the relation $\alpha_{\ell d}^{33} \simeq -5.8\,\alpha_{LQ}^{33}$, arising from the U_1 best fit WCs to the $R(D^{(*)})$ data. Branching ratios for $U_1 \to c\nu$, $b\tau$, $t\nu$ decays are fixed by the remaining ratio of coupling constants $r_{U_1} = (\alpha_{uN}^2/\alpha_{LQ}^{33})^2$, assuming no other channels are open. Blue dashed lines denote contours satisfying the U_1 best fit mass relation (3.7) for $\alpha_{LQ}^{33} = 0.15, 0.3, 0.5, 1.0$, and 2.0.

U_1 decay channels. In the minimal set-up we switch on only three couplings, $\alpha_{LQ}^{33}, \alpha_{ld}^{33}$ and α_{uN}^2, where α_{LQ}^{33} and α_{ld}^{33} are related through eq. (3.8), resulting in the branching ratios

$$\begin{aligned} \mathrm{Br}[U_1 \to t\bar{\nu}_\tau] : \mathrm{Br}[U_1 \to b\tau] : \mathrm{Br}[U_1 \to c\bar{N}_R] &= |\alpha_{LQ}^{33}|^2 : \left(|\alpha_{LQ}^{33}|^2 + |\alpha_{ld}^{33}|^2\right) : |\alpha_{uN}^2|^2 \\ &= \frac{0.03}{1+0.03r_{U_1}} : \frac{0.97}{1+0.03r_{U_1}} : \frac{0.03r_{U_1}}{1+0.03r_{U_1}}\,, \end{aligned} \tag{3.10}$$

where

$$r_{U_1} = \left(\frac{\alpha_{uN}^2}{\alpha_{LQ}^{33}}\right)^2. \tag{3.11}$$

Here, for simplicity, we have neglected the final state masses and the small corrections due to the off-diagonal CKM matrix elements in the $\alpha_{LQ}^{ij}\left(\bar{L}_L^i \gamma_\mu Q_L^j\right) U_1^{\mu\dagger}$. The presence of left-handed quark doublets also inevitably leads to CKM suppressed transitions $U_1 \to c\bar{\nu}_\tau, u\bar{\nu}_\tau, s\tau, d\tau$.

The corresponding LHC bounds for U_1 are shown in figure 5, assuming no other decay channels are open. The most stringent bounds come from $pp \to U_1 U_1$ pair production, with both leptoquarks decaying either as $U_1 \to cN_R$ [51] (grey region) or $U_1 \to b\tau$ [52] (brown region). Ref. [51] also gives bounds for the decay channel $U_1 \to t\nu_\tau$, which are not shown in figure 5 as they are always weaker in our setup. We see that direct searches still allow for $m_{U_1} \geq 1.5\,\mathrm{TeV}$, where the parameters of the model are still perturbative, as an explanation for the $R(D^{(*)})$ anomalies. It is worth noting that a simultaneous fit to all three decay channels by the experiments would improve the sensitivity to U_1; such an analysis is likely the most optimal strategy for discovering a U_1 state responsible for the $R(D^{(*)})$ anomalies.

Figure 5 also shows the constraint on the U_1 model parameter space from the CMS $pp \to \tau\tau$ search [53] (see also ATLAS search [54]). In orange is shown the constraint on r_{U_1}, as a function of m_{U_1}, that is obtained from figure 6 of ref. [13] with the replacement

JHEP02(2019)119

$g_U \to \left[(\alpha_{LQ}^{33})^2 + (\alpha_{ld}^{33})^2\right]^{1/2}$. Assuming the relation $\alpha_{\ell d}^{33} \simeq -5.8\,\alpha_{LQ}^{33}$, arising from the U_1 best fit WCs to the $R(D^{(*)})$ data, the bound on g_U in [13] translates to the excluded region in figure 5.

3.3 Scalar leptoquark S_1

The scalar leptoquark $S_1 \sim (\bar{3}, 1)_{1/3}$ has the following interaction Lagrangian,

$$\mathcal{L} \supset z_u (\bar{U}_R^c \ell_R) S_1 + z_d (\bar{d}_R^c N_R) S_1 + z_Q (\bar{Q}_L^c \epsilon L_L) S_1 . \tag{3.12}$$

Integrating out the leptoquark generates the following interaction Lagrangian above the electroweak scale

$$\begin{aligned} \mathcal{L}_{\text{eff}}^{S_1} = &- \frac{z_d z_u^*}{2m_{S_1}^2} Q_{\text{VR}} - \frac{z_d z_Q^*}{2m_{S_1}^2} \left(Q_{\text{SR}} - \frac{1}{4} Q_{\text{T}} \right) \\ &+ \frac{z_u z_Q^*}{2m_{S_1}^2} \left[\epsilon_{ab} (\bar{\ell}_R L_L^a)(\bar{u}_R Q_L^b) - \frac{1}{4} \epsilon_{ab} (\bar{\ell}_R \sigma_{\mu\nu} L_L^a)(\bar{u}_R \sigma^{\mu\nu} Q_L^b) \right] + \text{h.c.}, \end{aligned} \tag{3.13}$$

where the operators Q_{VR}, Q_{SR}, Q_{T} are defined in (2.3). The $b \to c\tau\bar{N}_R$ decay is generated if $z_u^{23} z_d^3 \neq 0$ or $z_Q^{23} z_d^3 \neq 0$. The two operators in the second line give rise to the $b \to c\tau\nu_i$ decay for $z_Q^{3i} z_u^{23} \neq 0$, where ν_i are the SM neutrinos, which interfere with the SM contribution; for simplicity, we therefore only consider the $b \to c\tau\bar{N}_R$ decay, setting $z_Q^{3i} = 0$, so that only the operators in the first line in (3.13) are generated (alternatively, one may consider the regime $z_u,\, z_Q \ll z_d$, so that the contribution from the second line is negligible).

In the analysis of collider constraints, we conservatively keep only the minimal set of S_1 couplings required for the $R(D^{(*)})$ anomaly nonzero: $z_u^{23}, z_d^3, z_Q^{23} \neq 0$. The Wilson coefficients of the $b \to c\tau\bar{N}_R$ operators $\mathcal{O}_{\text{VR}}$, $\mathcal{O}_{\text{SR}}$, $\mathcal{O}_{\text{T}}$ are given by,

$$\frac{c_{\text{VR}}}{\Lambda_{\text{eff}}^2} = -\frac{z_u^{23*} z_d^3}{2m_{S_1}^2}, \qquad \frac{c_{\text{SR}}^{(\mu)}}{\rho_{\text{SR}} \Lambda_{\text{eff}}^2} = -4 \frac{c_{\text{T}}^{(\mu)}}{\rho_{\text{T}} \Lambda_{\text{eff}}^2} = -\frac{z_Q^{23*} z_d^3}{2m_{S_1}^2}. \tag{3.14}$$

The best fit values for the S_1 WCs in table 2 then imply

$$m_{S_1} \simeq 1.2 \left| z_u^{23} z_d^3 \right|^{1/2} \left[\frac{40 \times 10^{-3}}{V_{cb}} \right]^{1/2} \text{TeV}\,, \tag{3.15}$$

with

$$z_u^{23} \simeq 1.1 z_Q^{23}. \tag{3.16}$$

using the lower set of best fits for S_1 in table 2 (the upper set is excluded by $B_c \to \tau\nu$, see figure 2). The branching ratios for S_1 decays are thus

$$\begin{aligned} \text{Br}[S_1 \to c\tau] : \text{Br}[S_1 \to b N_R] : \text{Br}[S_1 \to s\nu_\tau] &= \left(|z_u^{23}|^2 + |z_Q^{23}|^2 \right) : |z_d^3|^2 : |z_Q^{23}|^2 \\ &= \frac{0.69}{1 + 0.37 r_{S_1}} : \frac{0.37 r_{S_1}}{1 + 0.37 r_{S_1}} : \frac{0.31}{1 + 0.37 r_{S_1}}\,, \end{aligned} \tag{3.17}$$

JHEP02(2019)119

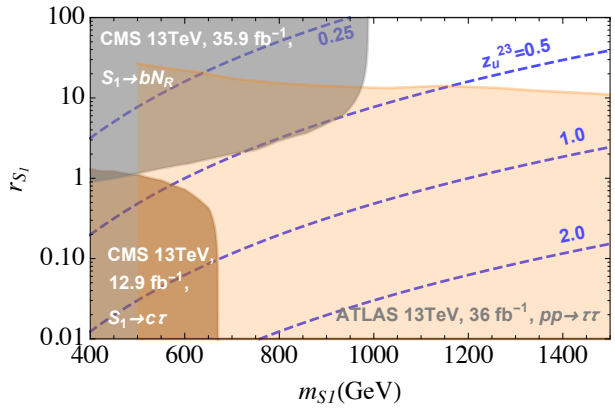

Figure 6. The LHC bounds from pair production of S_1 leptoquarks followed by $S_1 \to bN_R$ decays [51] (grey region) and $S_1 \to c\tau$ [52] (brown region), and from a recast of the ATLAS $pp \to \tau\tau$ search [54, 55] (orange region), as a function of m_{S_1} and the ratio $r_{S_1} = (z_d^3/z_u^{23})^2$ (3.18). The remaining ratio of coupling constants is fixed by the relation $z_u^{23} \simeq 1.1 z_Q^{23}$, arising from the S_1 best fit WCs to the $R(D^{(*)})$ data (2.14). Contours satisfying the S_1 best fit mass relation (3.15) are shown by blue dashed lines for $z_u^{23} = 0.25, 0.5, 1.0$, and 2.0.

where we have defined

$$r_{S_1} = \left(\frac{z_d^3}{z_u^{23}}\right)^2 . \tag{3.18}$$

The resulting bounds from $pp \to S_1 S_1$ pair production at the 13 TeV LHC are shown in figure 6. The grey shaded region is excluded by the CMS search [51] with 35.9 fb^{-1} integrated luminosity, assuming both S_1 decay as $S_1 \to bN_R$ with the branching ratio in (3.17). The brown shaded region is excluded by the CMS search [52] using 12.9 fb^{-1} integrated luminosity, assuming $pp \to S_1 S_1$ followed by $S_1 \to c\tau$ decay, with the r_{du} dependent branching ratio in (3.17). We have assumed the S_1 best fit mass relation (3.16) to $R(D^{(*)})$ data to derive these bounds.

The orange shaded region in figure 6 shows the 95% CL constraint from the recast of the 13 TeV ATLAS $pp \to \tau\tau$ search at 36^{-1} fb integrated luminosity [54], performed in ref. [55]. The bounds in figure 3 (left) in ref. [55] can be reinterpreted in terms of the S_1 model coupling to a right-handed neutrino by making the replacement $\lambda_{23}^L \to \left[(z_u^{23})^2 + (z_Q^{23})^2\right]^{1/2}$.

The combined set of constraints indicates that the S_1 leptoquark can be consistent with the $R(D^{(*)})$ anomaly for m_{S_1} as low as 1000 GeV, and with perturbative couplings (the required values of z_u^{23} are shown by dashed blue lines in figure 6).

3.4 Scalar leptoquark $\tilde{R}_2$

The scalar leptoquark $\tilde{R}_2 \sim (3,2)_{1/6}$ has the following interaction Lagrangian,

$$\mathcal{L} \supset \alpha_{Ld}\left(\bar{L}_L d_R\right)\epsilon \tilde{R}_2^\dagger + \alpha_{QN}\left(\bar{Q}_L N_R\right)\tilde{R}_2 + \text{h.c.}\,. \tag{3.19}$$

Integrating out the $\tilde{R}_2$ generates

$$\frac{c_{\text{SR}}^{(\mu)}}{\rho_{\text{SR}}\Lambda_{\text{eff}}^2} = 4\frac{c_{\text{T}}^{(\mu)}}{\rho_{\text{T}}\Lambda_{\text{eff}}^2} = \frac{\alpha_{Ld}^{33}\alpha_{QN}^2}{2m_{\tilde{R}_2}^2}. \tag{3.20}$$

JHEP02(2019)119

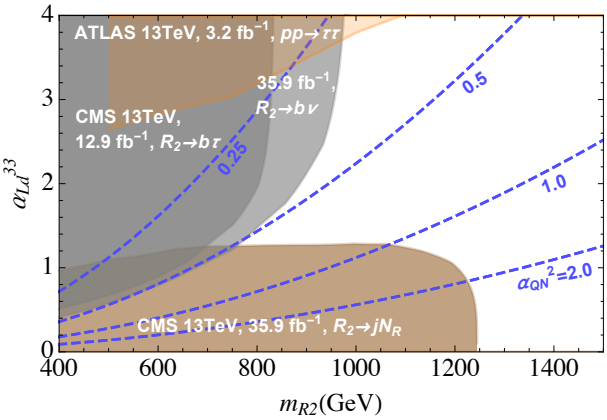

Figure 7. The LHC bounds from pair production of $\tilde{R}_2^{2/3}$ and $\tilde{R}_2^{-1/3}$ leptoquarks, for the decay channels $\tilde{R}_2^{2/3} \to b\bar{\tau}$ [52] (dark grey region), $\tilde{R}_2^{-1/3} \to b\bar{\nu}_\tau$ [51] (light grey region), $\tilde{R}_2^{2/3} \to cN_R$, $\tilde{R}_2^{-1/3} \to sN_R$ [51] (brown shaded region), and from t-channel exchange in $pp \to \tau\tau$ [13] (orange) as a function of $\tilde{R}_2$ mass and the coupling constant α_{Ld}^{33}. Contours satisfying the S_1 best fit mass relation (3.21) are shown by blue dashed lines, fixing $\alpha_{QN}^2 = 0.25, 0.5, 1.0$, and 2.0.

The best fit values for the $\tilde{R}_2$ WC in table 2 then imply

$$m_{\tilde{R}_2} \simeq 0.95 \left|\alpha_{Ld}^{33}\alpha_{QN}^2\right|^{1/2} \left[\frac{40\times10^{-3}}{V_{cb}}\right]^{1/2} \text{TeV}\,. \tag{3.21}$$

The leptoquark doublet $\tilde{R}_2$ contains two states: the charge $+2/3$ state $\tilde{R}_2^{2/3}$ and the charge $-1/3$ state $\tilde{R}_2^{-1/3}$. Keeping only the couplings relevant for the $R(D^{(*)})$ anomaly nonzero, $\alpha_{Ld}^{33}, \alpha_{QN}^2 \neq 0$, the $\tilde{R}_2$ states have two decay channels

$$\frac{\text{Br}[\tilde{R}_2^{2/3} \to b\bar{\tau}]}{\text{Br}[\tilde{R}_2^{2/3} \to cN_R]} = \frac{\text{Br}[\tilde{R}_2^{-1/3} \to b\bar{\nu}_\tau]}{\text{Br}[\tilde{R}_2^{-1/3} \to sN_R]} = \left(\frac{\alpha_{Ld}^{33}}{\alpha_{QN}^2}\right)^2, \tag{3.22}$$

where we have neglected differences due to the masses of the final state particles.

Assuming $\tilde{R}_2^{2/3}$ and $\tilde{R}_2^{-1/3}$ are degenerate, the LHC bounds from leptoquark pair production are shown in figure 7 as a function of $m_{\tilde{R}_2}$ and the α_{Ld}^{33} coupling. The remaining coupling, α_{QN}^2, is set by the $\tilde{R}_2$ best fit mass relation (3.21). We show bounds from LHC searches for all four decay channels: $\tilde{R}_2^{2/3} \to b\bar{\tau}$ [52] (dark grey region), $\tilde{R}_2^{-1/3} \to b\bar{\nu}_\tau$ [51] (light grey), and the combined $pp \to \tilde{R}_2^{2/3}\tilde{R}_2^{2/3*}$ and $pp \to \tilde{R}_2^{-1/3}\tilde{R}_2^{-1/3*}$ cross sections, followed by $\tilde{R}_2^{2/3} \to cN_R$ and $\tilde{R}_2^{-1/3} \to sN_R$ decays, which appear in the detector as 2j+MET [51] (brown shaded region). The orange shaded region shows the bounds from $pp \to \tau\tau$ searches [13], where $\tilde{R}_2$ can correct the tails of the distributions through the new t-channel exchange contribution. We see that $m_{\tilde{R}_2} \gtrsim 800\,\text{GeV}$ consistent with the $R(D^{(*)})$ anomaly is allowed, with perturbative couplings, even if no other decay channels are open.

4 Sterile neutrino phenomenology

In this section, we discuss the phenomenology associated with the right-handed (sterile) neutrino N_R. As we will see below, the coupling of N_R to the SM fermions through one of

JHEP02(2019)119

the higher dimension operators in eq. (2.8), needed to explain $R(D^{(*)})$, carries interesting implications for neutrino masses, cosmology, and collider signatures. We will assume that N_R is a Majorana fermion with mass $\lesssim \mathcal{O}(100)\,\text{MeV}$ so that it remains compatible with the measured missing invariant mass spectrum in the $\overline{B} \to D^{(*)}\tau\bar{\nu}$ decay chain. As in section 3, we do not consider the Φ model as it is excluded by $B_c \to \tau\nu$ constraints.

4.1 Neutrino masses

The effective operators (2.8) induce a N_R–ν_L Dirac mass at the two loop order via contributions of the form

$m_D \bar{N}_R \nu_L \sim$ 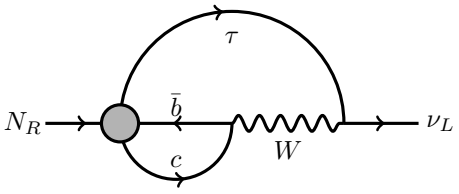

. (4.1)

Here, the simplified model mediator has been integrated out, producing an effective four-fermion vertex, shown in gray. Depending on the chiral structure of the simplified model, various mass insertions are mandated on the internal quark and lepton lines. In particular, the $\mathcal{O}_{\text{VR}}$ operator requires three mass insertions, while the scalar and tensor operators require only one. The corresponding Dirac masses can be estimated as

$$W': \quad m_D \sim \frac{c_{\text{VR}}}{\Lambda_{\text{eff}}^2}\frac{g_2^2}{2}\frac{V_{cb}}{(16\pi^2)^2} m_b m_c m_\tau \sim c_{\text{VR}} 10^{-3}\,\text{eV}, \tag{4.2a}$$

$$\tilde{R}_2: \quad m_D \sim c_{\text{SR}} m_b \frac{g_2^2}{2}\frac{V_{cb}}{(16\pi^2)^2} \sim c_{\text{SR}} 10^{2}\,\text{eV}, \tag{4.2b}$$

$$U_1: \quad m_D \sim \left[c_{\text{SL}} m_c + \frac{c_{\text{VR}}}{\Lambda_{\text{eff}}^2} m_b m_c m_\tau\right]\frac{g_2^2}{2}\frac{V_{cb}}{(16\pi^2)^2} \sim (c_{\text{SL}} 10^{2} + c_{\text{VR}} 10^{-3})\,\text{eV}, \tag{4.2c}$$

$$S_1: \quad m_D \sim \left[c_{\text{SR}} m_b + \frac{c_{\text{VR}}}{\Lambda_{\text{eff}}^2} m_b m_c m_\tau\right]\frac{g_2^2}{2}\frac{V_{cb}}{(16\pi^2)^2} \sim (c_{\text{SR}} 10^{2} + c_{\text{VR}} 10^{-3})\,\text{eV}\,. \tag{4.2d}$$

In the above estimates, we have ignored $\mathcal{O}(1)$ prefactors and loop integral factors apart from those implied by naïve dimensional analysis. Note that for diagrams with a single mass insertion, the Wilson coefficients c_{SL}, c_{SR} appear without the $1/\Lambda_{\text{eff}}^2$ prefactor. In such cases, strictly speaking, it is the couplings of the mediators rather than the Wilson coefficients that should appear in the estimates. However, since the collider constraints require mediators to be heavy, with mass approximately equal to Λ_{eff}, it is a reasonable approximation to use the Wilson coefficients everywhere in the above estimates.

Furthermore, for $\tilde{R}_2$, U_1, and S_1 mediators, which couple to the left-handed τ_L, there are additional two loop contributions to the neutrino mass matrix arising from the $\text{SU}(2)_L$ related operators involving ν_L. A representative diagram is shown in figure 8. While such diagrams contain similar mass insertions and WC scalings as the corresponding $c_{\text{SL,SR}}$ terms in eqs. (4.2), they are GIM suppressed and thus expected to produce only subleading corrections to the Dirac mass estimates in eqs. (4.2).

JHEP02(2019)119

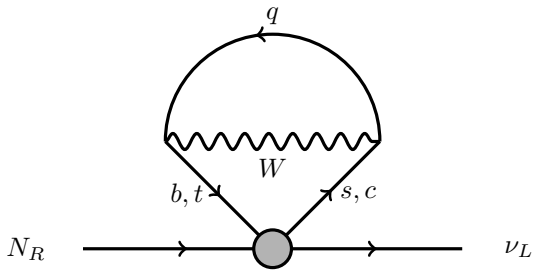

Figure 8. Dirac mass contribution by virtue of SU(2) counterparts of the four-Fermi operators that give rise to the $R(D^{(*)})$ enhancements. These diagrams are GIM suppressed and give subdominant contributions to the Dirac mass.

Since N_R is assumed to have a Majorana mass $m_{N_R} \lesssim 100\,\text{MeV}$, the contribution to the SM neutrino masses is $\sim m_D^2/m_{N_R}$, which should not exceed the observed neutrino mass scale $m_\nu \sim 0.1\,\text{eV}$. From the best fit regions shown in figures 2 or 3 (and the best fit values from table 2), it follows that the W'-mediated diagram gives a Dirac mass $m_D \sim 10^{-3}\,\text{eV}$, which is consistent with observed neutrino masses, whereas the R_2 mediated digram gives $m_D \sim 100\,\text{eV}$, which is in some tension for $m_{N_R} \lesssim 10\,\text{keV}$. Likewise, the U_1 and S_1 models produce similarly problematic contributions to the neutrino masses at their best fit points (see table 2). However, from figures 2 and 3 we also see that the 1σ CLs of the U_1 and S_1 models do contain regions with the scalar Wilson coefficients $|c_{\text{SL,SR}}| \ll 1$, corresponding to small couplings $\alpha_{LQ} \ll 1$ and $z_Q \ll 1$ (cf. eqs. (3.6) and (3.14)), which remain compatible with observed neutrino masses.

If additional operators are present, neutrino mass contributions can also be generated at one loop. For instance, as discussed in section 2.2, new operators coupling to second generation quark doublets can be introduced to cancel away large contributions to $b \to s\nu\bar{\nu}$ from the operators in eq. (2.11). Such 1-loop neutrino mass contributions scale as $m \sim \frac{1}{16\pi^2} m_f$ and, depending on whether the new operators couple to $\nu\nu$ or νN_R, contribute to the Majorana or Dirac mass terms for the neutrinos. Unless suppressed by small couplings in the diagram, such mass contributions are generally several orders of magnitude larger than what is allowed by the observed neutrino mass scale $m_\nu \sim 0.1\,\text{eV}$, and would need to be cancelled by fine-tuned values of bare neutrino masses.

Additional Dirac mass contributions beyond the diagrams considered above could worsen or improve the outlook. For instance, if the mediators also couple to other quarks, in particular the top quark, the corresponding two loop diagrams with a top quark mass insertion would lead to unacceptably large contributions to neutrino masses. On the other hand, additional Dirac mass terms that interfere destructively with the two loop contributions here could restore consistency in otherwise problematic regions of parameter space, albeit at the cost of some fine-tuning of parameters.

4.2 Sterile neutrino decay

The two loop diagrams considered above also give rise to the decay process $N_R \to \nu\gamma$ via the emission of a photon from one of the internal propagator lines (a representative diagram

JHEP02(2019)119

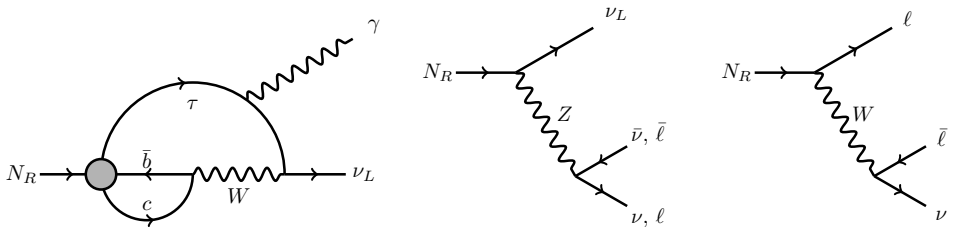

Figure 9. Sterile neutrino decay modes induced by the NP couplings (left) and by tree level sterile-active mixing (centre, right).

Model	$\Gamma_{N_R \to \nu\gamma}$	lifetime (s)
W'	$\frac{c_{\rm VR}^2}{\Lambda_{\rm eff}^4} \frac{\alpha}{32\,\pi^8} V_{cb}^2 G_F^2 m_\tau^2 m_b^2 m_c^2 m_{N_R}^3$	$c_{\rm VR}^{-2}\, 10^{24}\, (m_{N_R}/\text{keV})^{-3}$
$\tilde{R}_2$	$c_{\rm SR}^2 \frac{\alpha}{32\,\pi^8} V_{cb}^2 G_F^2 m_b^2 m_{N_R}^3$	$c_{\rm SR}^{-2}\, 10^{13}\, (m_{N_R}/\text{keV})^{-3}$
U_1	$c_{\rm SL}^2 \frac{\alpha}{32\,\pi^8} V_{cb}^2 G_F^2 m_c^2 m_{N_R}^3$	$c_{\rm SL}^{-2}\, 10^{14}\, (m_{N_R}/\text{keV})^{-3}$
S_1	$c_{\rm SR}^2 \frac{\alpha}{32\,\pi^8} V_{cb}^2 G_F^2 m_b^2 m_{N_R}^3$	$c_{\rm SR}^{-2}\, 10^{13}\, (m_{N_R}/\text{keV})^{-3}$

Table 3. Approximate $N_R \to \nu\gamma$ decay rates (middle column) and lifetimes (final column) for the mediators listed in the first column. For $U_1(S_1)$, we only show the contribution from the $c_{\rm SL}(c_{\rm SR})$ operators, which are expected to dominate; if these coefficients vanish, the decay rates and lifetimes get contributions from $c_{\rm VR}$ of the same form as that for the W' operator.

is shown in figure 9 (left)). The approximate $N_R \to \nu\gamma$ decay rates[1] for the simplified models, along with the corresponding decay lifetime estimates, are listed in table 3 (for related calculations, see refs. [56–59]). Note that for a given mediator and sterile neutrino mass m_{N_R}, the decay rate is completely fixed by the Wilson coefficients consistent with the $R(D^{(*)})$ anomaly.

For appreciable mixing between N_R and the SM neutrinos, the leading tree-level decay is into three SM neutrinos (figure 9 center) and, if kinematically accessible, into charged leptons (figure 9 right). The $N_R \to 3\nu$ decay rate is

$$\Gamma_{N_R \to 3\nu} \simeq \frac{G_F^2}{192\,\pi^3} m_{N_R}^5 \sin^2\theta \simeq 10^{-48} \left(\frac{m_{N_R}}{\text{keV}}\right)^5 \left(\frac{\sin^2\theta}{10^{-4}}\right) \text{GeV}, \tag{4.3}$$

where θ is the mixing angle between N_R and the SM neutrino. The $N_R \to 3\nu$ decay width is in general subdominant to the $N_R \to \nu\gamma$ decay width induced by the $R(D^{(*)})$ anomaly. For a direct comparison, one can rewrite the $N_R \to \nu\gamma$ decay rate in table 3 in terms of the Dirac mass from eq. 4.2, then convert to the mixing angle via $\sin\theta \approx m_D/m_N$. For instance, for S_1 this gives $\Gamma(N \to \nu\gamma) \sim 32\,\alpha\,\sin^2\theta\, m_N^5\, G_F^2/\pi^4/g^4$. Thus

$$\frac{\Gamma(N \to \nu\gamma)_{S_1}}{\Gamma(N_R \to 3\nu)_{S_1}} \approx \frac{32 \times 192\,\alpha}{\pi\, g^4} \sim 10^3. \tag{4.4}$$

[1]The mass insertion required by the helicity flip for the emission of a photon can occur on an internal fermion line, and does not incur the cost of a mass suppression on an external fermion leg, in contrast to $f_1 \to f_2\gamma$ diagrams via an $\text{SU}(2)_L$ electroweak loop.

JHEP02(2019)119

4.3 Sterile neutrino cosmology

The above estimates imply that the sterile neutrino N_R can be fairly long-lived. The interactions with SM fermions mandated by consistency with the $R(D^{(*)})$ anomaly also lead to copious production of N_R in the early Universe. The cosmological aspects of the sterile neutrino therefore require careful treatment.

The interactions with SM fermions thermalize the N_R population with the SM bath at high temperatures. These interactions are active until the temperature drops below the masses of the SM fermions involved in these interactions, i.e., around the GeV scale. Since we have assumed $m_{N_R} \lesssim 100\,\text{MeV}$, the N_R abundance is not Boltzmann suppressed, and N_R survives as an additional relativistic neutrino species in the early Universe. It then becomes crucial to determine the fate of this N_R population.

For the $\tilde{R}_2$, U_1, and S_1 mediated models, it follows from table 3 that the N_R lifetime is $\sim 10^{14}(m_{N_R}/\text{keV})^{-3}\,\text{s}$. For $m_{N_R} \sim \mathcal{O}(\text{eV–keV})$, this implies a late decay of the N_R population into the $\gamma\nu$ channel, which injects an unacceptable amount of photons into the diffuse photon background. The exception are masses close to the upper limit of the range we consider, $m_{N_R} \lesssim 100\,\text{MeV}$, for which the lifetime is reduced to $\lesssim 1\,\text{s}$. The decays then occur before big bang nucleosynthesis (BBN) and do not leave any visible imprints.

In contrast, for the W' mediated case (or for U_1, S_1 in the parts of the Wilson coefficient 1σ CL regions where c_{SL}, c_{SR} are vanishingly small), the lifetime is much longer because of the additional mass insertions in the decay diagrams, and a lifetime $\lesssim 1\text{s}$ cannot be achieved for any realistic choices of parameters. However, for $m_{N_R} \lesssim 100\,\text{keV}$, the sterile neutrino has a lifetime greater than the age of the Universe and could in principle form a component of dark matter or dark radiation.

The dark matter and dark radiation possibilities of N_R in the W' model have been extensively discussed in ref. [17]. In contrast to traditionally studied frameworks of sterile neutrino dark matter, where the relic abundance is produced via freeze-in mechanisms (see, e.g., [60–65]), the W' model involves the sterile neutrino freezing out as a relativistic species, leading to too large of a relic abundance for masses greater than $\mathcal{O}(\text{keV})$. This can be fixed with appropriate entropy dilution from, for instance, late decays of GeV scale sterile neutrinos [58, 58, 66, 67], which also makes the dark matter colder, improving compatibility with warm dark matter constraints. The γ-ray bounds from various observations [68] rule out dark matter lifetimes of $\mathcal{O}(10^{26\text{–}28})\,\text{s}$ in the keV–MeV window, ruling out the case that N_R constitutes all of dark matter. This leaves us with the possibility that N_R may constitutes a small fraction — at the sub-percent level — of dark matter. Future γ-ray observations will probe this possibility and could discover a line signal from the $N_R \to \gamma\nu$ decay. For masses $m_{N_R} \lesssim \text{keV}$, N_R can act as dark radiation and contribute to the effective number of relativistic degrees of freedom $\Delta N_{\text{eff}} \approx \mathcal{O}(0.1)$ at BBN and/or CMB decoupling, which could be detected with future instruments such as CMB-S4 [69]. Lifetimes shorter than the age of the Universe, however, are incompatible with current observational constraints.

JHEP02(2019)119

4.4 Displaced decays at direct searches and colliders

As discussed in the previous section, in the $\tilde{R}_2$, U_1, and S_1 models, cosmology favors the regime $m_{N_R} \sim 100\,\text{MeV}$, with a lifetime $\lesssim 1\,\text{s}$. Since the dominant decay channel is $N_R \to \nu\gamma$, this would give rise to displaced decays into a photon+MET. Such displaced signals could provide an interesting, but challenging, target for proposed detectors such as SHiP [70], MATHUSLA [71], FASER [72], and CODEX-b [73]. Displaced decays can also occur in the W' UV completion of refs. [16, 17], where, as discussed earlier, GeV scale sterile neutrinos with lifetimes $\lesssim 1\,\text{s}$ might be needed to entropy dilute problematic overabundances of the N_R; these can also lead to several other observable signals at various direct and cosmological probes (see, e.g., the discussion in [74]).

5 Conclusions

We have performed an EFT study of the lowest dimension electroweak operators that can account for the $R(D^{(*)})$ anomalies, assuming they arise because of incoherent contributions from semitauonic decays involving a right-handed sterile neutrino N_R. These dimension-six operators can arise from a tree-level mediator exchange in five possible simplified models. We examined the fits and constraints for each simplified model. While all five models have 1σ fit regions consistent with the $R(D^{(*)})$ data, the case of the scalar doublet mediator is conservatively in tension with constraints from $\text{Br}[B_c \to \tau\nu]$, while the experimental bounds on $b \to s\nu\bar{\nu}$ rates are in tension with the predicted rates from the scalar leptoquark $\tilde{R}_2$.

The fit regions of the remaining three simplified models imply sizable semileptonic branching ratios for the tree-level mediators. We find that each model already faces fairly stringent collider constraints. The searches for the W' mediator in the $W' \to \tau\nu$ channel exclude the model for perturbative couplings, where the calculations are reliable, with the possible exception of very light W' masses (see figure 4 and surrounding discussion). The two leptoquark models are consistent with LHC search results provided the mediator masses are $\mathcal{O}(\text{TeV})$, while their couplings may still remain in the perturbative regime. Our analysis indicates promising paths to future discovery of the tree-level mediators at the LHC, with couplings and masses consistent with the fit to the $R(D^{(*)})$ data. The vector leptoquark U_1^μ can best be probed at the LHC with simultaneous fits to the three decays $U_1 \to cN_R, U_1 \to b\tau$ and $U_1 \to t\nu_\tau$. Likewise, the scalar leptoquark S_1 can be probed via $S_1 \to bN_R$ and $S_1 \to c\tau$ decays. Since the mediators cannot be arbitrarily heavy if the couplings are to remain perturbative, prospects of detecting them at the LHC are quite encouraging.

We have also discussed the phenomenology associated with the sterile neutrino N_R. In simplified models involving $\tilde{R}_2$, U_1, and S_1, constraints from contributions to neutrino masses as well as cosmology indicate a preference for $m_{N_R} \sim 10$–$100\,\text{MeV}$ with a decay lifetime $\lesssim 1\,\text{s}$ in the dominant channel $N_R \to \nu\gamma$. This opens up the potential for detecting displaced decays of N_R at various detectors. It also implies potentially measurable distortions of the kinematical distributions in semileptonic B meson decays due to the heavy sterile neutrino in the final state. For the W' simplified model, the predicted contribution to neutrino masses is much smaller and poses no constraints on the model. The

JHEP02(2019)119

predicted decay lifetime of N_R is correspondingly much longer than the age of the Universe. Consequently, a significant relic abundance of N_R is likely present in the universe, which can contribute to dark radiation and give measurable deviations to the effective number of relativistic degrees of freedom $\Delta N_{\rm eff} \approx \mathcal{O}(0.1)$ at BBN and/or CMB decoupling for $m_{N_R} \lesssim$ keV, or constitute a small fraction of dark matter for N_R in the keV–MeV mass range with possible gamma ray signals at future probes.

The interpretation of the $R(D^{(*)})$ anomaly in terms of new physics coupling the SM fermions to a right-handed sterile neutrino is therefore an exciting possibility with testable predictions in multiple directions, spanning kinematic distributions of the measured B meson decays, searches for heavy TeV scale particles at the LHC, displaced decay signals at various detectors, as well as astrophysical and cosmological signatures.

Acknowledgments

We thank Damir Bečirević, Florian Bernlochner, Admir Greljo, Svjetlana Fajfer, Nejc Košnik for helpful discussions and communications about their work. JZ acknowledges support in part by the DOE grant DE-SC0011784. BS was partially supported by the NSF CAREER grant PHY1654502. This work was performed in part at the Aspen Center for Physics, which is supported by National Science Foundation grant PHY-1066293. DR thanks Florian Bernlochner, Stephan Duell, Zoltan Ligeti and Michele Papucci for their ongoing collaboration in the development of `Hammer`, which was used for part of the analysis in this work. The work of DR was supported in part by NSF grant PHY-1720252.

A Differential distributions

In this appendix we collect the predictions for several normalized differential distributions for $\overline{B} \to (D^* \to D\pi)(\tau \to \ell\bar{\nu}_\ell\nu_\tau)\bar{\nu}$ and $\overline{B} \to D(\tau \to \ell\bar{\nu}_\ell\nu_\tau)\bar{\nu}$ decay chains, shown in the left and right columns in figures 10–13, respectively. In each plot, the SM predictions (blue dashed curves) are compared with the predictions for the particular simplified model (grey bands), obtained by varying the relevant Wilson coefficients over the 2σ regions in figure 2. In each of the figures the first row shows the normalized distribution $(1/\Gamma)(d\Gamma/dE_D)$, where E_D is the energy of the outgoing D meson in the B meson rest frame. The second row contains the $(1/\Gamma)(d\Gamma/dE_\ell)$ distribution, with E_ℓ the energy of the final state charged lepton, while the third row shows the $(1/\Gamma)(d\Gamma/dm^2_{\rm miss})$ distribution, with $m^2_{\rm miss}$ the combined invariant mass of the system of three final state neutrinos. The final row in each figure shows the $(1/\Gamma)(d\Gamma/d\cos\theta_{D\ell})$ normalized distribution, where $\theta_{D\ell}$ is the angle between the three momenta of the D meson and the charged lepton, ℓ, in the rest frame of the B meson.

The comparison between the SM predictions (blue dashed curves) and the predictions for the W' simplified model (grey bands) is shown in figure 10. The differences between the two predictions are small, below about 10% for $(1/\Gamma)(d\Gamma/dE_\ell)$ and well below this for the other distributions. Similarly small corrections from NP to the shapes of distributions are found for the $\tilde{R}_2$ model, figure 11. In this case the largest deviation is found for the $(1/\Gamma)(d\Gamma/dE_D)$ distribution for the $\overline{B} \to D^* \to D\pi$ decay (figure 11, first row, right panel)

JHEP02(2019)119

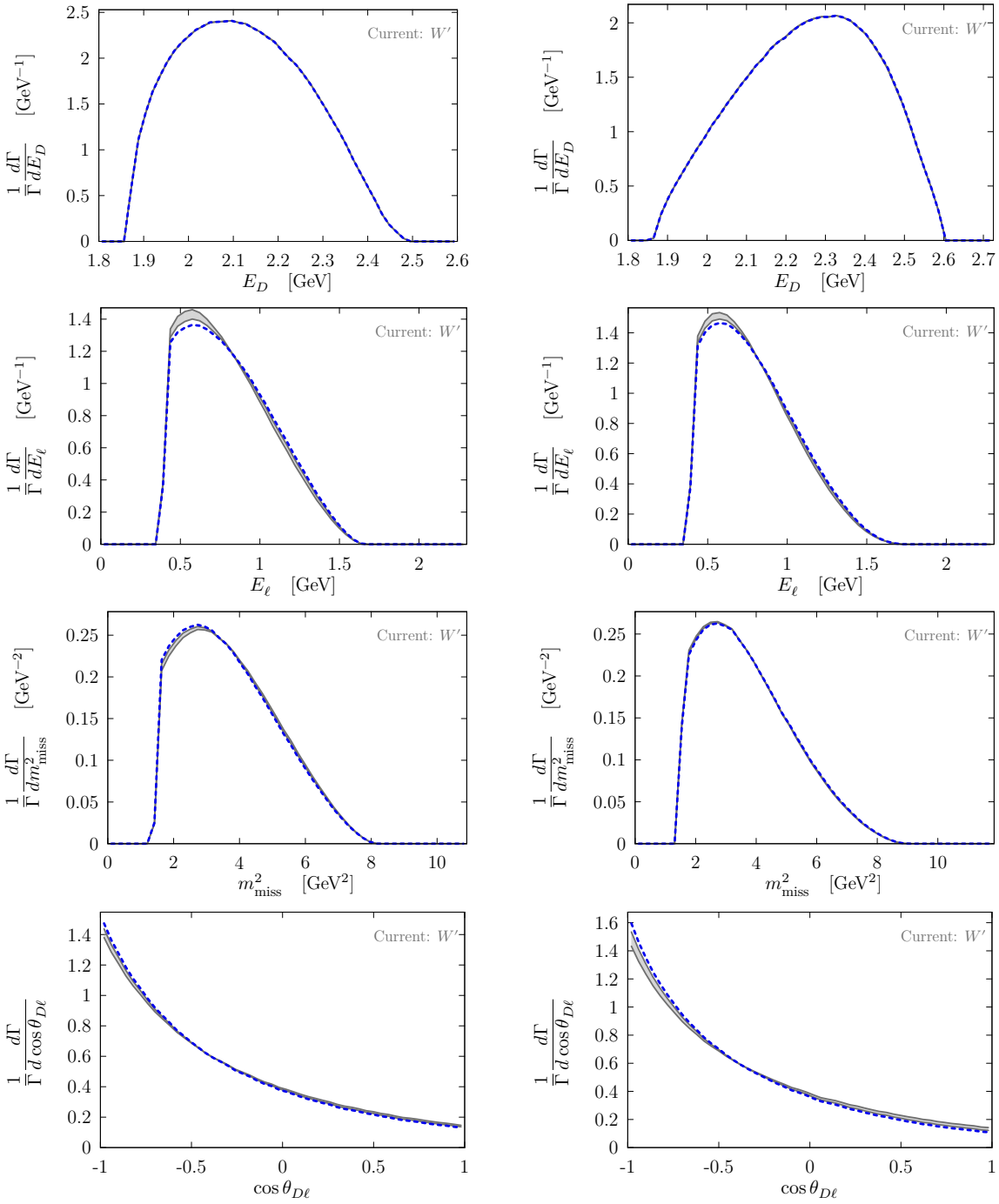

Figure 10. Gray bands show kinematic distributions for $\overline{B} \to (D^* \to D\pi)(\tau \to \ell\bar{\nu}_\ell\nu_\tau)\bar{\nu}$ (left) and $\overline{B} \to D(\tau \to \ell\bar{\nu}_\ell\nu_\tau)\bar{\nu}$ (right) in the B rest frame for the W' simplified model in table 1, with the Wilson coefficient $c_{\rm VR}$ ranging over 2σ best fit regions in figure 2, and applying the phase space cuts (2.20). The blue dashed curves show the SM prediction.

and is at the level of about $\mathcal{O}(20\%)$. The deviations are potentially sizable for the U_1 and S_1 models for at least some of the distributions, see figures 12 and 13, respectively.

JHEP02(2019)119

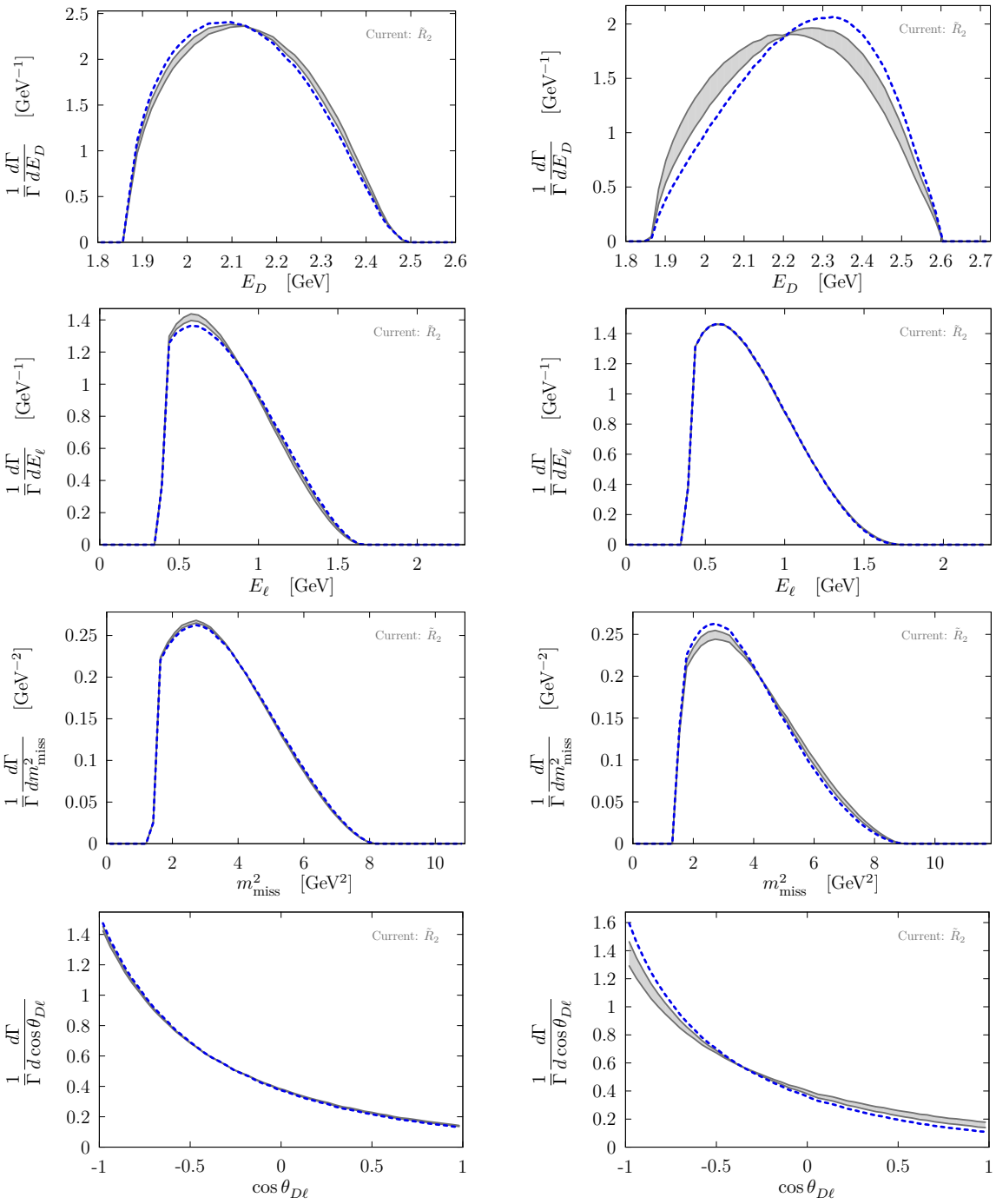

Figure 11. Gray bands show kinematic distributions for $\overline{B} \to (D^* \to D\pi)(\tau \to \ell\bar{\nu}_\ell\nu_\tau)\bar{\nu}$ (left) and $\overline{B} \to D(\tau \to \ell\bar{\nu}_\ell\nu_\tau)\bar{\nu}$ (right) in the B rest frame for the $\tilde{R}_2$ simplified model in table 1, with the Wilson coefficients $c_{\rm SR} = 4c_{\rm T}$ ranging over 2σ best fit regions in figure 2, and applying the phase space cuts (2.20). The blue dashed curves show the SM prediction.

JHEP02(2019)119

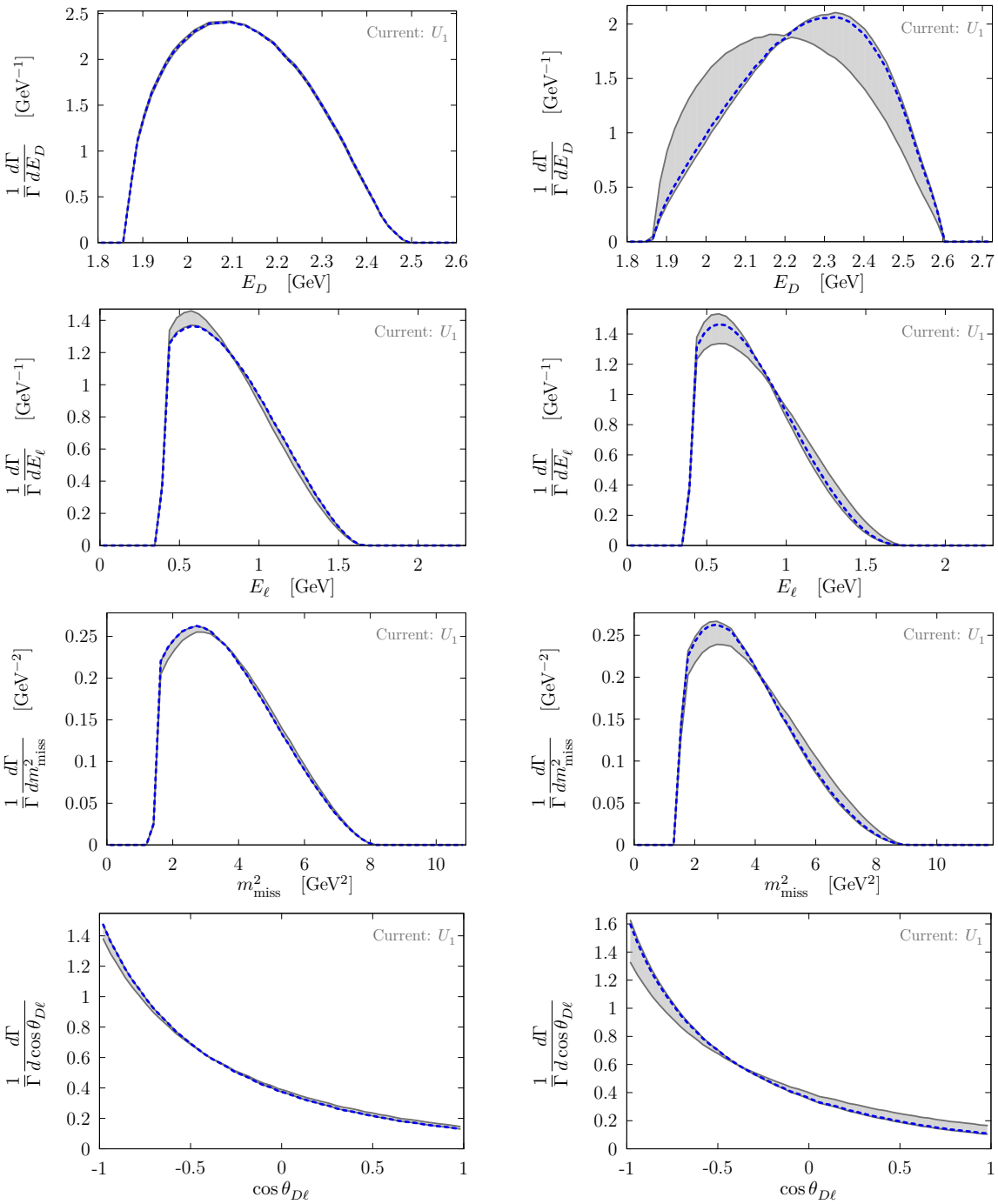

Figure 12. Gray bands show kinematic distributions for $\overline{B} \to (D^* \to D\pi)(\tau \to \ell\bar{\nu}_\ell\nu_\tau)\bar{\nu}$ (left) and $\overline{B} \to D(\tau \to \ell\bar{\nu}_\ell\nu_\tau)\bar{\nu}$ (right) in the B rest frame for the U_1 simplified model in table 1, with the Wilson coefficients $c_{\rm SL}, c_{\rm VR}$ ranging over 2σ best fit regions in figure 2, and applying the phase space cuts (2.20). The blue dashed curves show the SM prediction.

JHEP02(2019)119

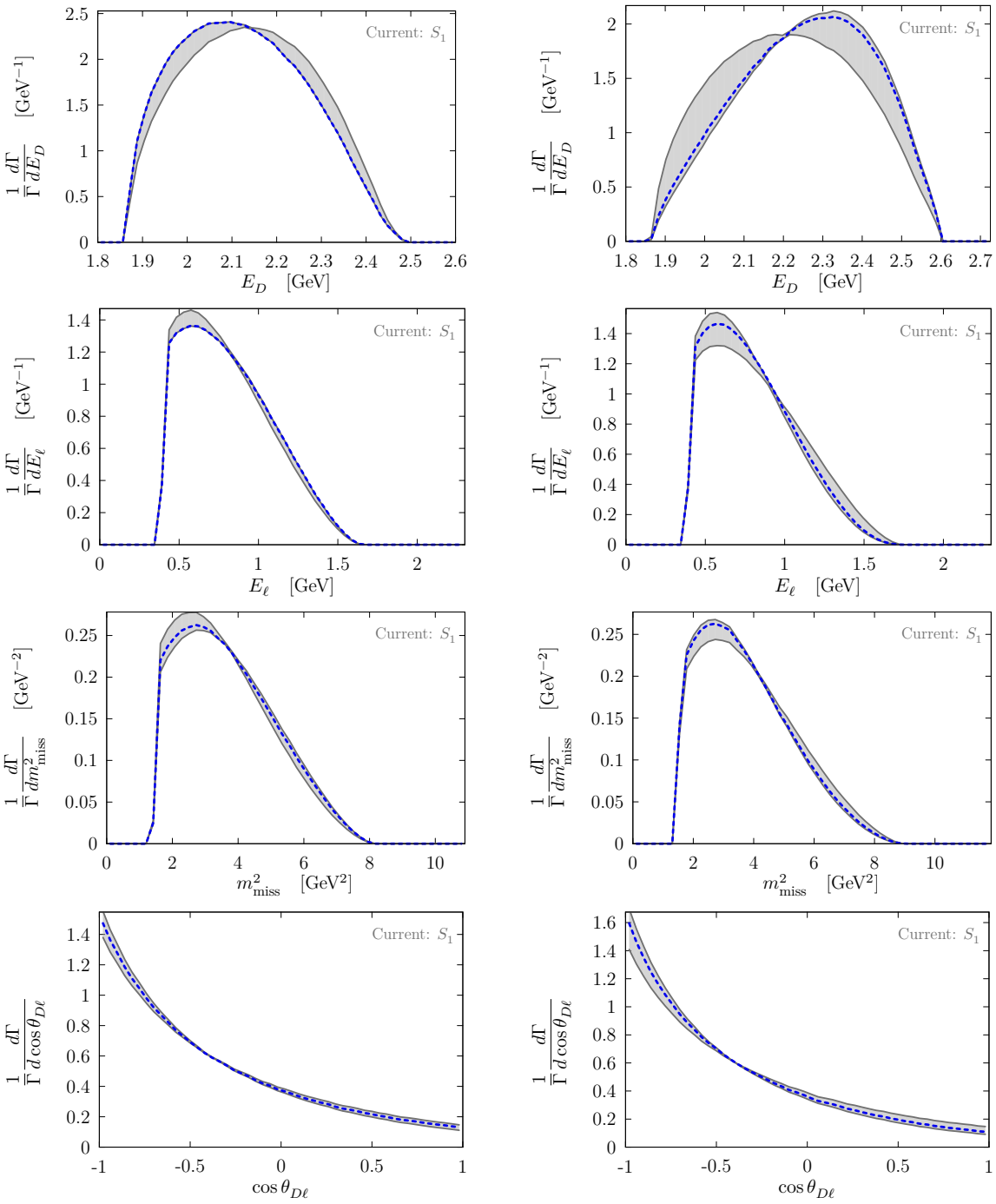

Figure 13. Gray bands show kinematic distributions for $\overline{B} \to (D^* \to D\pi)(\tau \to \ell\bar{\nu}_\ell\nu_\tau)\bar{\nu}$ (left) and $\overline{B} \to D(\tau \to \ell\bar{\nu}_\ell\nu_\tau)\bar{\nu}$ (right) in the B rest frame for the S_1 simplified model in table 1, with the Wilson coefficients $c_{\rm VR}, c_{\rm SR} = -4c_T$ ranging over 2σ best fit regions in figure 2, and applying the phase space cuts (2.20). The blue dashed curves show the SM prediction.

JHEP02(2019)119

References

[1] BaBar collaboration, *Evidence for an excess of $\bar{B} \to D^{(*)}\tau^-\bar{\nu}_\tau$ decays*, *Phys. Rev. Lett.* **109** (2012) 101802 [arXiv:1205.5442] [INSPIRE].

[2] BaBar collaboration, *Measurement of an Excess of $\bar{B} \to D^{(*)}\tau^-\bar{\nu}_\tau$ Decays and Implications for Charged Higgs Bosons*, *Phys. Rev.* **D 88** (2013) 072012 [arXiv:1303.0571] [INSPIRE].

[3] Belle collaboration, *Measurement of the branching ratio of $\bar{B} \to D^{(*)}\tau^-\bar{\nu}_\tau$ relative to $\bar{B} \to D^{(*)}\ell^-\bar{\nu}_\ell$ decays with hadronic tagging at Belle*, *Phys. Rev.* **D 92** (2015) 072014 [arXiv:1507.03233] [INSPIRE].

[4] Belle collaboration, *Measurement of the branching ratio of $\bar{B}^0 \to D^{*+}\tau^-\bar{\nu}_\tau$ relative to $\bar{B}^0 \to D^{*+}\ell^-\bar{\nu}_\ell$ decays with a semileptonic tagging method*, in proceedings of the *51st Rencontres de Moriond on Electroweak Interactions and Unified Theories*, La Thuile, Italy, 12–19 March 2016, arXiv:1603.06711 [INSPIRE].

[5] Belle collaboration collaboration, *Measurement of the τ lepton polarization in the decay $\bar{B} \to D^*\tau^-\bar{\nu}_\tau$*, arXiv:1608.06391 [INSPIRE].

[6] LHCb collaboration, *Measurement of the ratio of branching fractions $\mathcal{B}(\bar{B}^0 \to D^{*+}\tau^-\bar{\nu}_\tau)/\mathcal{B}(\bar{B}^0 \to D^{*+}\mu^-\bar{\nu}_\mu)$*, *Phys. Rev. Lett.* **115** (2015) 111803 [*Erratum ibid.* **115** (2015) 159901] [arXiv:1506.08614] [INSPIRE].

[7] HFLAV collaboration, *Averages of b-hadron, c-hadron and τ-lepton properties as of summer 2016*, *Eur. Phys. J.* **C 77** (2017) 895 [arXiv:1612.07233] [INSPIRE].

[8] F.U. Bernlochner, Z. Ligeti, M. Papucci and D.J. Robinson, *Combined analysis of semileptonic B decays to D and D^*: $R(D^{(*)})$, $|V_{cb}|$ and new physics*, *Phys. Rev.* **D 95** (2017) 115008 [arXiv:1703.05330] [INSPIRE].

[9] D. Bigi, P. Gambino and S. Schacht, *$R(D^*)$, $|V_{cb}|$ and the Heavy Quark Symmetry relations between form factors*, *JHEP* **11** (2017) 061 [arXiv:1707.09509] [INSPIRE].

[10] S. Jaiswal, S. Nandi and S.K. Patra, *Extraction of $|V_{cb}|$ from $B \to D^{(*)}\ell\nu_\ell$ and the Standard Model predictions of $R(D^{(*)})$*, *JHEP* **12** (2017) 060 [arXiv:1707.09977] [INSPIRE].

[11] A.K. Alok, D. Kumar, S. Kumbhakar and S.U. Sankar, *D^* polarization as a probe to discriminate new physics in $\bar{B} \to D^*\tau\bar{\nu}$*, *Phys. Rev.* **D 95** (2017) 115038 [arXiv:1606.03164] [INSPIRE].

[12] S. Bhattacharya, S. Nandi and S.K. Patra, *Looking for possible new physics in $B \to D^{(*)}\tau\nu_\tau$ in light of recent data*, *Phys. Rev.* **D 95** (2017) 075012 [arXiv:1611.04605] [INSPIRE].

[13] D.A. Faroughy, A. Greljo and J.F. Kamenik, *Confronting lepton flavor universality violation in B decays with high-p_T tau lepton searches at LHC*, *Phys. Lett.* **B 764** (2017) 126 [arXiv:1609.07138] [INSPIRE].

[14] F. Feruglio, P. Paradisi and A. Pattori, *Revisiting Lepton Flavor Universality in B Decays*, *Phys. Rev. Lett.* **118** (2017) 011801 [arXiv:1606.00524] [INSPIRE].

[15] F. Feruglio, P. Paradisi and A. Pattori, *On the Importance of Electroweak Corrections for B Anomalies*, *JHEP* **09** (2017) 061 [arXiv:1705.00929] [INSPIRE].

JHEP02(2019)119

[16] P. Asadi, M.R. Buckley and D. Shih, *It's all right(-handed neutrinos): a new W' model for the $R_{D^{(*)}}$ anomaly*, *JHEP* **09** (2018) 010 [arXiv:1804.04135] [INSPIRE].

[17] A. Greljo, D.J. Robinson, B. Shakya and J. Zupan, *$R(D^{(*)})$ from W' and right-handed neutrinos*, *JHEP* **09** (2018) 169 [arXiv:1804.04642] [INSPIRE].

[18] X.-G. He and G. Valencia, *B decays with τ leptons in nonuniversal left-right models*, *Phys. Rev.* **D 87** (2013) 014014 [arXiv:1211.0348] [INSPIRE].

[19] X.-G. He and G. Valencia, *Lepton universality violation and right-handed currents in $b \to c\tau\nu$*, *Phys. Lett.* **B 779** (2018) 52 [arXiv:1711.09525] [INSPIRE].

[20] S. Fajfer, J.F. Kamenik, I. Nisandzic and J. Zupan, *Implications of Lepton Flavor Universality Violations in B Decays*, *Phys. Rev. Lett.* **109** (2012) 161801 [arXiv:1206.1872] [INSPIRE].

[21] D. Bečirević, S. Fajfer, N. Košnik and O. Sumensari, *Leptoquark model to explain the B-physics anomalies, R_K and R_D*, *Phys. Rev.* **D 94** (2016) 115021 [arXiv:1608.08501] [INSPIRE].

[22] G. Cvetič, F. Halzen, C.S. Kim and S. Oh, *Anomalies in (semi)-leptonic B decays $B^\pm \to \tau^\pm\nu$, $B^\pm \to D\tau^\pm\nu$ and $B^\pm \to D^*\tau^\pm\nu$ and possible resolution with sterile neutrino*, *Chin. Phys.* **C 41** (2017) 113102 [arXiv:1702.04335] [INSPIRE].

[23] X.-Q. Li, Y.-D. Yang and X. Zhang, *Revisiting the one leptoquark solution to the $R(D^{(*)})$ anomalies and its phenomenological implications*, *JHEP* **08** (2016) 054 [arXiv:1605.09308] [INSPIRE].

[24] R. Alonso, B. Grinstein and J. Martin Camalich, *Lifetime of B_c^- Constrains Explanations for Anomalies in $B \to D^{(*)}\tau\nu$*, *Phys. Rev. Lett.* **118** (2017) 081802 [arXiv:1611.06676] [INSPIRE].

[25] A. Celis, M. Jung, X.-Q. Li and A. Pich, *Scalar contributions to $b \to c(u)\tau\nu$ transitions*, *Phys. Lett.* **B 771** (2017) 168 [arXiv:1612.07757] [INSPIRE].

[26] G. Buchalla, A.J. Buras and M.E. Lautenbacher, *Weak decays beyond leading logarithms*, *Rev. Mod. Phys.* **68** (1996) 1125 [hep-ph/9512380] [INSPIRE].

[27] M. Freytsis, Z. Ligeti and J.T. Ruderman, *Flavor models for $\bar{B} \to D^{(*)}\tau\bar{\nu}$*, *Phys. Rev.* **D 92** (2015) 054018 [arXiv:1506.08896] [INSPIRE].

[28] I. Doršner, S. Fajfer, N. Košnik and I. Nišandžić, *Minimally flavored colored scalar in $\bar{B} \to D^{(*)}\tau\bar{\nu}$ and the mass matrices constraints*, *JHEP* **11** (2013) 084 [arXiv:1306.6493] [INSPIRE].

[29] I. Doršner, S. Fajfer, A. Greljo, J.F. Kamenik and N. Košnik, *Physics of leptoquarks in precision experiments and at particle colliders*, *Phys. Rept.* **641** (2016) 1 [arXiv:1603.04993] [INSPIRE].

[30] Z. Ligeti, M. Papucci and D.J. Robinson, *New Physics in the Visible Final States of $B \to D^{(*)}\tau\nu$*, *JHEP* **01** (2017) 083 [arXiv:1610.02045] [INSPIRE].

[31] HPQCD collaboration, *B-meson decay constants: a more complete picture from full lattice QCD*, *Phys. Rev.* **D 91** (2015) 114509 [arXiv:1503.05762] [INSPIRE].

[32] Particle Data Group collaboration, *Review of Particle Physics*, *Chin. Phys.* **C 40** (2016) 100001 [INSPIRE].

JHEP02(2019)119

[33] J.F. Kamenik and C. Smith, *Tree-level contributions to the rare decays $B^+ \to \pi^+ \nu\bar{\nu}$, $B^+ \to K^+ \nu\bar{\nu}$, and $B^+ \to K^{*+} \nu\bar{\nu}$ in the Standard Model*, *Phys. Lett.* **B 680** (2009) 471 [arXiv:0908.1174] [INSPIRE].

[34] J.F. Kamenik and C. Smith, *FCNC portals to the dark sector*, *JHEP* **03** (2012) 090 [arXiv:1111.6402] [INSPIRE].

[35] PARTICLE DATA GROUP collaboration, *Review of Particle Physics*, *Phys. Rev.* **D 98** (2018) 030001 [INSPIRE].

[36] A.J. Buras, J. Girrbach-Noe, C. Niehoff and D.M. Straub, *$B \to K^{(*)} \nu\bar{\nu}$ decays in the Standard Model and beyond*, *JHEP* **02** (2015) 184 [arXiv:1409.4557] [INSPIRE].

[37] F. Bernlochner, S. Duell, Z. Ligeti, M. Papucci and D.J. Robinson, *Hammer: Helicity amplitude module for matrix element reweighting*, in preparation (2018).

[38] ATLAS collaboration, *Search for High-Mass Resonances Decaying to $\tau\nu$ in pp Collisions at $\sqrt{s} = 13$ TeV with the ATLAS Detector*, *Phys. Rev. Lett.* **120** (2018) 161802 [arXiv:1801.06992] [INSPIRE].

[39] CMS collaboration, *Search for a W' boson decaying to a τ lepton and a neutrino in proton-proton collisions at $\sqrt{s} = 13$ TeV*, submitted to Phys. Lett. (2018), arXiv:1807.11421 [INSPIRE].

[40] CMS collaboration, *Search for heavy gauge W' boson in events with an energetic lepton and large missing transverse momentum at $\sqrt{s} = 13$ TeV*, *Phys. Lett.* **B 770** (2017) 278 [arXiv:1612.09274] [INSPIRE].

[41] CMS collaboration, *Search for W' decaying to tau lepton and neutrino in proton-proton collisions at $\sqrt{s} = 13$ TeV*, CMS-PAS-EXO-16-006 (2016) [INSPIRE].

[42] L. Di Luzio and M. Nardecchia, *What is the scale of new physics behind the B-flavour anomalies?*, *Eur. Phys. J.* **C 77** (2017) 536 [arXiv:1706.01868] [INSPIRE].

[43] A. Greljo, J. Martin Camalich and J.D. Ruiz-Álvarez, *The Mono-Tau Menace: From B Decays to High-p_T Tails*, arXiv:1811.07920 [INSPIRE].

[44] CMS collaboration, *Search for low mass vector resonances decaying into quark-antiquark pairs in proton-proton collisions at $\sqrt{s} = 13$ TeV*, *JHEP* **01** (2018) 097 [arXiv:1710.00159] [INSPIRE].

[45] CMS collaboration, *Search for narrow resonances in dijet final states at $\sqrt{s} = 8$ TeV with the novel CMS technique of data scouting*, *Phys. Rev. Lett.* **117** (2016) 031802 [arXiv:1604.08907] [INSPIRE].

[46] CMS collaboration, *Search for dijet resonances in proton-proton collisions at $\sqrt{s} = 13$ TeV and constraints on dark matter and other models*, *Phys. Lett.* **B 769** (2017) 520 [*Corrigendum ibid.* **B 772** (2017) 882] [arXiv:1611.03568] [INSPIRE].

[47] ATLAS collaboration, *Search for New Physics in Dijet Mass and Angular Distributions in pp Collisions at $\sqrt{s} = 7$ TeV Measured with the ATLAS Detector*, *New J. Phys.* **13** (2011) 053044 [arXiv:1103.3864] [INSPIRE].

[48] CDF collaboration, *Search for new particles decaying to dijets at CDF*, *Phys. Rev.* **D 55** (1997) R5263 [hep-ex/9702004] [INSPIRE].

[49] S. Knapen and D.J. Robinson, *Disentangling Mass and Mixing Hierarchies*, *Phys. Rev. Lett.* **115** (2015) 161803 [arXiv:1507.00009] [INSPIRE].

JHEP02(2019)119

[50] I. Doršner and A. Greljo, *Leptoquark toolbox for precision collider studies*, *JHEP* **05** (2018) 126 [arXiv:1801.07641] [INSPIRE].

[51] CMS collaboration, *Constraints on models of scalar and vector leptoquarks decaying to a quark and a neutrino at* $\sqrt{s} = 13$ *TeV*, CMS-PAS-SUS-18-001 (2018) [INSPIRE].

[52] CMS collaboration, *Search for third-generation scalar leptoquarks and heavy right-handed neutrinos in final states with two tau leptons and two jets in proton-proton collisions at* $\sqrt{s} = 13$ *TeV*, *JHEP* **07** (2017) 121 [arXiv:1703.03995] [INSPIRE].

[53] ATLAS collaboration, *Search for Minimal Supersymmetric Standard Model Higgs bosons* H/A *and for a* Z' *boson in the* $\tau\tau$ *final state produced in pp collisions at* $\sqrt{s} = 13$ *TeV with the ATLAS Detector*, *Eur. Phys. J.* **C 76** (2016) 585 [arXiv:1608.00890] [INSPIRE].

[54] ATLAS collaboration, *Search for additional heavy neutral Higgs and gauge bosons in the ditau final state produced in* $36\,fb^{-1}$ *of pp collisions at* $\sqrt{s} = 13$ *TeV with the ATLAS detector*, *JHEP* **01** (2018) 055 [arXiv:1709.07242] [INSPIRE].

[55] T. Mandal, S. Mitra and S. Raz, $R_{D^{(*)}}$ *in minimal leptoquark scenarios: impact of interference on the exclusion limits from LHC data*, arXiv:1811.03561 [INSPIRE].

[56] L. Lavoura, *General formulae for* $f_1 \to f_2\gamma$, *Eur. Phys. J.* **C 29** (2003) 191 [hep-ph/0302221] [INSPIRE].

[57] G.-G. Wong, *New gauge bosons in an asymmetric left-right model*, *Phys. Rev.* **D 46** (1992) 3987 [INSPIRE].

[58] F. Bezrukov, H. Hettmansperger and M. Lindner, *keV sterile neutrino Dark Matter in gauge extensions of the Standard Model*, *Phys. Rev.* **D 81** (2010) 085032 [arXiv:0912.4415] [INSPIRE].

[59] A. Aparici, J. Herrero-Garcia, N. Rius and A. Santamaria, *On the Nature of the Fourth Generation Neutrino and its Implications*, *JHEP* **07** (2012) 030 [arXiv:1204.1021] [INSPIRE].

[60] S. Dodelson and L.M. Widrow, *Sterile-neutrinos as dark matter*, *Phys. Rev. Lett.* **72** (1994) 17 [hep-ph/9303287] [INSPIRE].

[61] X.-D. Shi and G.M. Fuller, *A New dark matter candidate: Nonthermal sterile neutrinos*, *Phys. Rev. Lett.* **82** (1999) 2832 [astro-ph/9810076] [INSPIRE].

[62] B. Shakya, *Sterile Neutrino Dark Matter from Freeze-In*, *Mod. Phys. Lett.* **A 31** (2016) 1630005 [arXiv:1512.02751] [INSPIRE].

[63] B. Shakya and J.D. Wells, *Sterile Neutrino Dark Matter with Supersymmetry*, *Phys. Rev.* **D 96** (2017) 031702 [arXiv:1611.01517] [INSPIRE].

[64] S.B. Roland, B. Shakya and J.D. Wells, *Neutrino Masses and Sterile Neutrino Dark Matter from the PeV Scale*, *Phys. Rev.* **D 92** (2015) 113009 [arXiv:1412.4791] [INSPIRE].

[65] B. Shakya and J.D. Wells, *Exotic Sterile Neutrinos and Pseudo-Goldstone Phenomenology*, arXiv:1801.02640 [INSPIRE].

[66] R.J. Scherrer and M.S. Turner, *Decaying Particles Do Not Heat Up the Universe*, *Phys. Rev.* **D 31** (1985) 681 [INSPIRE].

[67] T. Asaka, M. Shaposhnikov and A. Kusenko, *Opening a new window for warm dark matter*, *Phys. Lett.* **B 638** (2006) 401 [hep-ph/0602150] [INSPIRE].

JHEP02(2019)119

[68] R. Essig, E. Kuflik, S.D. McDermott, T. Volansky and K.M. Zurek, *Constraining Light Dark Matter with Diffuse X-Ray and Gamma-Ray Observations*, *JHEP* **11** (2013) 193 [arXiv:1309.4091] [INSPIRE].

[69] CMB-S4 collaboration, *CMB-S4 Science Book, First Edition*, arXiv:1610.02743 [INSPIRE].

[70] SHiP collaboration, *A facility to Search for Hidden Particles (SHiP) at the CERN SPS*, arXiv:1504.04956 [INSPIRE].

[71] J.P. Chou, D. Curtin and H.J. Lubatti, *New Detectors to Explore the Lifetime Frontier*, *Phys. Lett.* **B 767** (2017) 29 [arXiv:1606.06298] [INSPIRE].

[72] J.L. Feng, I. Galon, F. Kling and S. Trojanowski, *ForwArd Search ExpeRiment at the LHC*, *Phys. Rev.* **D 97** (2018) 035001 [arXiv:1708.09389] [INSPIRE].

[73] V.V. Gligorov, S. Knapen, M. Papucci and D.J. Robinson, *Searching for Long-lived Particles: A Compact Detector for Exotics at LHCb*, *Phys. Rev.* **D 97** (2018) 015023 [arXiv:1708.09395] [INSPIRE].

[74] M. Drewes and B. Garbrecht, *Combining experimental and cosmological constraints on heavy neutrinos*, *Nucl. Phys.* **B 921** (2017) 250 [arXiv:1502.00477] [INSPIRE].

JHEP02(2019)119